

RANDOM BATCH METHODS FOR DISCRETIZED PDES ON GRAPHS

MARTÍN HERNÁNDEZ[†] AND ENRIQUE ZUAZUA^{*†‡}

ABSTRACT. Gas transport and other complex real-world challenges often require solving and controlling partial differential equations (PDEs) defined on graph structures, which typically demand substantial memory and computational resources. The Random Batch Method (RBM) offers significant relief from these demands by enabling the simulation of large-scale systems with reduced computational cost.

In this paper, we analyze the application of RBM for solving PDEs on one-dimensional graphs, specifically concentrating on the heat equation. Our approach involves a two-step process: initially discretizing the PDE to transform it into a finite-dimensional problem, followed by the application of the RBM. We refer to this integrated approach as *discretize+RBM*.

We establish the convergence of this method in expectation, under the appropriate selection and simultaneous reduction of the switching parameter in RBM and the discretization parameters.

Moreover, we extend these findings to include the optimal control of the heat equation on graphs, enhancing the practical utility of our methodology.

The efficacy and computational efficiency of our proposed solution are corroborated through numerical experiments that not only demonstrate convergence but also show significant reductions in computational costs.

Our algorithm can be viewed as a randomized variant of domain decomposition, specifically adapted for PDEs defined on graph structures. It is sufficiently versatile to be applied to a wide range of linear PDEs – not just the heat equation – while maintaining comparable analytical guarantees and convergence properties.

CONTENTS

1. Introduction	2
1.1. Motivation	2
1.2. Main Contribution	2
1.3. Related Work	2
1.4. Outline	3
2. Preliminaries	3
2.1. The Finite Element Method	3
2.2. Overview of the RBM	4
3. Approximation by the Random Batch Method	6
3.1. Approximation of the Heat Equation via the RBM	6
3.2. Application to Optimal Control	8
4. The RBM for the Heat Equation on Networks	10
4.1. The Heat Equation on Graphs	10
4.2. Numerical Simulations	12
5. Conclusions and Open Problems	20
Acknowledgments	21
References	22

2020 *Mathematics Subject Classification.* 65C99, 65M55, 65M75, 35R02.

Key words and phrases. Random Batch Methods, Numerical Methods, Partial Differential Equations on Graphs, Heat Equation, Optimal Control.

[†] Chair for Dynamics, Control, Machine Learning, and Numerics, Alexander von Humboldt-Professorship, Department of Mathematics, Friedrich-Alexander-Universität Erlangen-Nürnberg, 91058 Erlangen, Germany.

^{*} Departamento de Matemáticas, Universidad Autónoma de Madrid, 28049 Madrid, Spain.

[‡] Chair of Computational Mathematics, University of Deusto. Av. de las Universidades, 24, 48007 Bilbao, Basque Country, Spain.

1. INTRODUCTION

1.1. Motivation. The simulation of complex models such as gas transport in extensive pipeline networks is often computationally demanding and resource-intensive [28, 25]. Developing efficient algorithms that can deliver faster solutions while reducing resource consumption is crucial. A notable advancement in this field is the Random Batch Method (RBM), which was originally introduced to efficiently simulate large-scale interacting particle systems [14]. RBM achieves efficiency by randomly grouping particles into small batches and computing their interactions within brief time subintervals. This method of breaking down complex problems into simpler, manageable subproblems is fundamental to RBM's success and can be applied across various domains. The Mini-Batch Gradient Descent algorithm in machine learning, which strikes a balance between computational efficiency and model performance, employs a similar approach [3, Section 3].

RBM is also adaptable to high-dimensional linear dynamical systems, where it involves decomposing the governing matrix into smaller sub-matrices. The time interval is partitioned into subintervals, during each of which a randomly selected batch of sub-matrices defines a randomized dynamical system. As shown in [31], the solution of this random system converges in expectation to the solution of the original system when the subintervals are sufficiently small. This methodology has been proven effective for optimal-control problems as well [31].

1.2. Main Contribution. In this paper, we extend the RBM to address partial differential equations (PDEs) and their associated optimal control problems. Our approach, which we term *discretize+RBM*, begins with the spatial discretization of PDEs, converting them into finite-dimensional dynamical systems, followed by the application of RBM. This method necessitates a careful convergence analysis, which depends on the appropriate selection of discretization and randomization parameters.

Control theory cautions that the initial discretization of a system prior to the application of control strategies can lead to the generation of high-frequency spurious solutions [9, 10, 11]. This phenomenon is particularly relevant in hyperbolic wave-like systems, where it can lead to divergence and stability issues. Consequently, in the current framework, both the discretization and RBM methodologies must be meticulously calibrated and coordinated to circumvent such instabilities. This necessitates a thorough analysis to ensure that the discretization does not introduce anomalies that could amplify under the RBM's stochastic dynamics.

Our focus in this article is primarily on the one-dimensional heat equation on a graph. We employ the Finite Element Method (FEM) for spatial discretization, followed by the application of RBM. We establish that a careful selection of both the time subinterval size for RBM and the spatial mesh size for FEM ensures the convergence of the combined FEM+RBM methodology. This convergence is then extended to quadratic optimal control problems.

We validate our analytical results through numerical experiments that not only confirm convergence but also demonstrate the computational efficiency of our approach. Our method can be viewed as a randomized version of the classical domain or graph decomposition methods applied to matrix decompositions in discrete dynamics. Additionally, partitioning the problem into small batches not only lowers memory requirements by handling subproblems independently but also leverages the inherent structure of the system for parallelization. This parallel execution further accelerates computations, contributing to a significant reduction in total computational time.

Although our primary focus is on the heat equation and the FEM discretization scheme, the principles underlying our *discretize+RBM* methodology are applicable to other linear PDEs, higher-dimensional settings, and various discretization techniques. This versatility highlights the potential of our approach as a broadly applicable tool for efficiently solving and controlling PDEs in complex domains.

1.3. Related Work. The RBM was initially proposed for finite-dimensional interacting particle systems, leading to the development of convergence guarantees [15] and the management of antisymmetric interactions [16]. The approach has been expanded to linear dynamical systems integrating it with Model Predictive Control (MPC), providing convergence estimates [17, 30]. The stochastic process model introduced by [21] represents another adaptation of the RBM concept, demonstrating convergence as the step size diminishes.

The application of RBM to PDEs includes analyses on particle-interacting systems' mean-field limits [13] and on the homogeneous Landau and Fokker-Planck equations [4, 24]. These studies employ RBM to approximate PDEs through interacting particle systems. Our approach, however, directly utilizes

classical PDE discretization methods such as FEM. Other methodologies that combine discretization with randomization include the work of [7] on parabolic PDEs and [5] on gradient flows, both offering insights into convergence behaviors under various conditions.

1.4. Outline. The remainder of this article is structured as follows: Section 2 introduces our model and outlines the FEM for the one-dimensional heat equation, along with a detailed description of the RBM, as discussed in [31]. Section 3 is devoted to presenting our main findings on convergence for PDE optimal control. Section 4 presents numerical simulations to validate our results and illustrate the efficacy of the random graph decomposition approach.

2. PRELIMINARIES

Let us first consider $L, T > 0$ and the following one-dimensional heat equation:

$$\begin{cases} \partial_t y - \partial_{xx} y = f, & (x, t) \in (0, L) \times (0, T), \\ y(0, t) = y(L, t) = 0, & t \in (0, T), \\ y(x, 0) = y^0(x), & x \in (0, L). \end{cases} \quad (2.1)$$

Here, $y^0 \in L^2(0, L)$ is the initial condition, and $f \in L^2(0, T; H^{-1}(0, L))$ is a source term. According to [8, Section 7.1.2], the existence and uniqueness of the solution $y \in C((0, T); L^2(0, L)) \cap L^2(0, T; H_0^1(0, L))$ for (2.1) are guaranteed.

2.1. The Finite Element Method. In this section, we introduce FEM to semi-discretize (2.1).

Consider a spatial mesh step $h = L/(N + 1)$ with $N \in \mathbb{N}$, so that the partition defined by the nodes

$$x_j = jh, \quad j \in \{0, \dots, N + 1\}, \quad (2.2)$$

decomposes the interval $[0, L]$ into $N + 1$ subintervals of length h . Let us introduce the continuous piecewise linear functions $\phi_j(x)$, such that $\phi_j(x_l) = \delta_{jl}$ for $j \in \{1, \dots, N\}$ and $l \in \{0, \dots, N + 1\}$, where δ denotes the Kronecker delta. We define the finite-element space V_h as the span of $\{\phi_j\}_{j=1}^N$.

Assume that $y^0 \in H_0^1(0, L)$, and denote by y_h^0 the projection of y^0 onto V_h with respect to the scalar product of $H_0^1(0, L)$ (see [26, Section 3.5]). Consider the semi-discrete (variational) formulation of (2.1) as follows: Find $y_h \in C^1(0, T; V_h)$ such that

$$\begin{cases} \int_0^L \partial_t y_h(x, t) \phi_j(x) dx + \int_0^L \partial_x y_h(x, t) \partial_x \phi_j(x) dx = \int_0^L f(x, t) \phi_j(x) dx, \\ \int_0^L y_h(x, 0) \phi_j(x) dx = \int_0^L y^0(x) \phi_j(x) dx, \end{cases} \quad (2.3)$$

for every $t \in (0, T)$ and $j \in \{1, \dots, N\}$. According to [26, Proposition 11.2.1], the following theorem holds.

Theorem 2.1. *Assume that $y^0 \in H_0^1(0, L)$ and $f \in L^2(0, T; L^2(0, L))$. Let y be the solution of (2.1) and y_h the solution of (2.3) given by (2.5). Then, there exists a constant $C > 0$, independent of $h > 0$, such that*

$$\|y(t) - y_h(t)\|_{L^2(0, L)}^2 \leq Ch^4 \left(\|y^0\|_{H_0^1(0, L)}^2 + \|f\|_{L^2(0, T; L^2(0, L))}^2 \right), \quad (2.4)$$

for every $t \in (0, T)$.

Observe that (2.3) defines a system of ordinary differential equations. Indeed, since $y_h \in C^1(0, T; V_h)$, the semi-discrete solution can be written as

$$y_h(x, t) = \sum_{j=1}^N y_j(t) \phi_j(x), \quad (2.5)$$

with coefficients $y_j \in C^1(0, T)$ and the corresponding finite-dimensional state $\mathbf{y}_h(t) = (y_1(t), \dots, y_N(t))$ solves

$$\begin{cases} E_h \partial_t \mathbf{y}_h + R_h \mathbf{y}_h = \mathbf{f}_h, & t \in (0, T), \\ E_h \mathbf{y}_h(0) = \mathbf{y}_h^0, \end{cases} \quad (2.6)$$

where the mass and stiffness matrices $E_h, R_h \in \mathbb{R}^{N \times N}$ are given by

$$E_h(j, k) = \int_0^L \phi_j(x) \phi_k(x) dx, \quad R_h(j, k) = \int_0^L \partial_x \phi_j(x) \partial_x \phi_k(x) dx,$$

for $j, k \in \{1, \dots, N\}$, and \mathbf{y}_h^0 and \mathbf{f}_h are defined component-wise as

$$y_j^0 = \int_0^L y^0(x) \phi_j(x) dx, \quad \text{and} \quad f_j = \int_0^L f(x) \phi_j(x) dx,$$

respectively. In the present setting, these matrices can be computed explicitly and take the form:

$$E_h = h \begin{pmatrix} 2/3 & 1/6 & 0 & \cdots & 0 \\ 1/6 & \ddots & \ddots & \ddots & \vdots \\ 0 & \ddots & \ddots & \ddots & 0 \\ \vdots & \ddots & \ddots & \ddots & 1/6 \\ 0 & \cdots & 0 & 1/6 & 2/3 \end{pmatrix}, \quad R_h = \frac{1}{h} \begin{pmatrix} 2 & -1 & 0 & \cdots & 0 \\ -1 & \ddots & \ddots & \ddots & \vdots \\ 0 & \ddots & \ddots & \ddots & 0 \\ \vdots & \ddots & \ddots & \ddots & -1 \\ 0 & \cdots & 0 & -1 & 2 \end{pmatrix}. \quad (2.7)$$

Of course, this finite-dimensional interpretation of the FEM approximation of the heat equation can be extended to the multi-dimensional setting in arbitrary domains, although, in that case, the matrix representation is not that explicit.

2.2. Overview of the RBM. In this section, we provide an introduction to the RBM, following [31], in the context of (2.6). We first apply the RBM to approximate the heat equation numerically, and then consider an optimal control problem.

Consider the time step $\delta = T/(K+1) > 0$, for $K \in \mathbb{N}$. We define the time intervals $[(k-1)\delta, k\delta]$ for each $k \in \{1, \dots, K\}$. Let $M > 0$ be a positive integer and introduce a family of identically and independently distributed random variables $\{\omega_k\}_{k=1}^K$, each taking values in $\{1, \dots, 2^M\}$. For each $k \in \{1, \dots, K\}$, we denote by $p_i \in [0, 1]$ the probability that ω_k equals $i \in \{1, \dots, 2^M\}$. We assume that

$$\sum_{i=1}^{2^M} p_i = 1,$$

and we denote by $\boldsymbol{\omega}$ the vector

$$\boldsymbol{\omega} = (\omega_1, \dots, \omega_K) \in \{1, \dots, 2^M\}^K.$$

This induces a random variable with values in $\mathcal{P}(\{1, \dots, M\})$, where \mathcal{P} denotes the power set. Indeed, for each $S_i \in \mathcal{P}(\{1, \dots, M\})$ with $i \in \{1, \dots, 2^M\}$, when $\omega_k = i$, the random variable S_{ω_k} takes the value S_i . Hence, the probability law of S_{ω_k} is entirely derived from that of ω_k .

This random setting allows us to introduce a random dynamic system as follows: Let $R_h \in \mathbb{R}^{N \times N}$ be the matrix in (2.7), and consider a decomposition of R_h into sub-matrices $\{R_{h,m}\}_{m=1}^M$ such that

$$R_h = \sum_{m=1}^M R_{h,m}. \quad (2.8)$$

Then, for each time interval $[(k-1)\delta, k\delta]$, we randomly select a set of indices S_{ω_k} and define the corresponding random, time-dependent matrix

$$R_{rb}(\boldsymbol{\omega}, t) = \sum_{m \in S_{\omega_k}} \frac{R_{h,m}}{\pi_m}, \quad t \in [(k-1)\delta, k\delta], \quad (2.9)$$

for each $k \in \{1, \dots, K\}$. Here, π_m , given by

$$\pi_m := \sum_{i \in \{j \in \{1, \dots, 2^M\} : m \in S_j\}} p_i,$$

is a normalization constant ensuring that $\mathbb{E}[R_{rb}] = R_h$. In the following, we assume that $\pi_m > 0$ for every $m \in \{1, \dots, M\}$ (as in [31]). Observe that the matrix R_{rb} is piecewise constant with respect to time and randomly switches at each time step.

Remark 2.1 (On the choice of decomposition and sampling sets). *Although the abstract framework allows for the decomposition of the stiffness matrix R_h into $M = N^2$ scalar 1×1 submatrices $R_{h,m}$ – one per entry of R_h – this choice is computationally impractical.*

Instead, we partition the matrix $R_h \in \mathbb{R}^{N \times N}$ into a smaller number of rectangular blocks such that the decomposition (2.8) holds. For instance, one may consider four submatrices $R_{h,m}$, each containing a nonzero block of approximate size $(N/2) \times (N/2)$. As a result, we typically choose $M \ll N$ in practice.

Similarly, the random variable ω_k need not take values in the full set $1, \dots, 2^M$. Instead, we may assign positive probability only to a subset of interest – usually much smaller than 2^M – by setting $p_i = 0$ for all other values.

As shown in Section 4, when R_h arises from the discretization of a PDE on a graph, the block partition has a natural geometric interpretation: each edge contributes one block. In our numerical experiments, we cluster the edges into three groups, thereby defining three large blocks and, consequently, three submatrices $R_{h,1}$, $R_{h,2}$, and $R_{h,3}$ (i.e., $M = 3$). We then assign positive probability only to the singleton subsets $S_1 = 1$, $S_2 = 2$, and $S_3 = 3$ (see Figure 1).

This minimalist strategy ensures that $\pi_m > 0$ for all $m \in 1, \dots, M$. Therefore, over each time interval $[(k-1)\delta, k\delta)$, the matrix $R_{rb}(\omega, t)$ randomly selects one of the matrices $R_{h,1}$, $R_{h,2}$, or $R_{h,3}$.

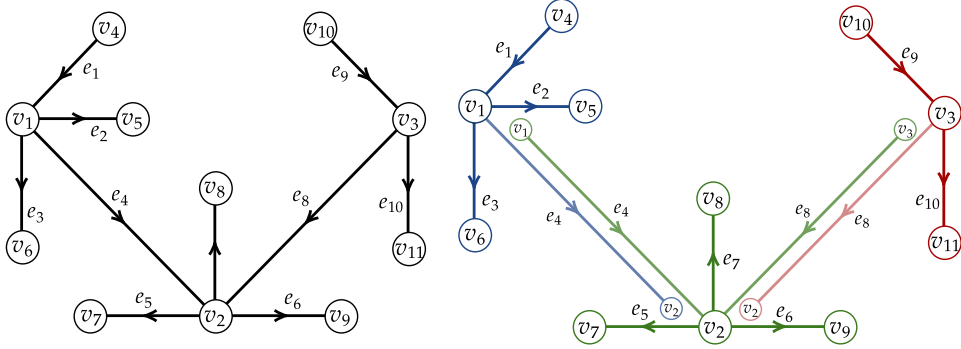


FIGURE 1. Illustration of a graph decomposition into three edge groups (shown in different colors). Each group is associated with one block of the stiffness matrix. Since edges e_4 and e_8 belong to two groups, the chosen block overlaps.

Now, we consider the following random dynamical system:

$$\begin{cases} E_h \partial_t \mathbf{y}_R(\omega, t) + R_{rb}(\omega, t) \mathbf{y}_R(\omega, t) = \mathbf{f}_h, & t \in (0, T), \\ E_h \mathbf{y}_R(0) = \mathbf{y}_h^0, \end{cases} \quad (2.10)$$

where \mathbf{y}_h^0 and \mathbf{f}_h are the same initial condition and source term as in (2.6), respectively.

Following [31], we can prove that $\mathbf{y}_R(\omega, t)$ approximates the solution \mathbf{y}_h of equation (2.6) in expectation as $\delta \rightarrow 0$. Specifically, setting

$$\text{Var}[R_{rb}] := \sum_{i=1}^{2^M} \left(\left\| R_h - \sum_{m \in S_i} \frac{R_{h,m}}{\pi_m} \right\|^2 p_i \right), \quad (2.11)$$

where $\|\cdot\|$ denotes the l^2 -norm, the following theorem holds:

Theorem 2.2. *Let \mathbf{y}_h and \mathbf{y}_R denote the solutions of (2.6) and (2.10), respectively. Then, for every $t \in (0, T)$, we have*

$$\mathbb{E} [\|\mathbf{y}_h(t) - \mathbf{y}_R(t)\|^2] \leq (\|E_h^{-1} R_h\| T^2 + 2T) (\|E_h^{-1} \mathbf{y}_h^0\| + \|E_h^{-1} \mathbf{f}_h\|_{L^1(0, T; \mathbb{R}^N)})^2 \frac{\text{Var}[R_{rb}]}{\lambda_{\min}^2(E_h)} \delta, \quad (2.12)$$

where $\lambda_{\min}(E_h)$ denotes the minimum eigenvalues of E_h .

Remark 2.2. *Regarding the previous theorem, the following comments are in order:*

1. In [31, Theorem 1], the matrix E_h is considered as the identity matrix. However, since E_h is invertible, by multiplying (2.10) by E_h^{-1} , and considering that $\|E_h^{-1}\| = (\lambda_{\min}(E_h))^{-1}$, estimation (2.12) follows.
2. In this approach, we choose to keep the matrix E_h in (2.6) instead of multiplying the system by E_h^{-1} , which would yield an equivalent system with the dynamics matrix $E_h^{-1}R_h$. Therefore, Theorem 2.2 could be applied in this setting as well. However, note that, in the first case, namely, in the setting we have chosen, the matrix to be decomposed is R_h , whereas in the second one, it would be $E_h^{-1}R_h$. Our primary motivation for the first choice, decomposing R_h , is to keep the analogy with the RBM for PDEs on graphs. When dealing with the discretization of PDEs on graphs, both R_h and E_h exhibit a block diagonal structure, each block corresponding to the dynamics on a subgraph (see Section 4.1). Therefore, leveraging domain decomposition, a natural decomposition of R_h can be achieved by utilizing submatrices associated to each block. In contrast, when we chose the second approach, due to the presence of the matrix $E_h^{-1}R_h$, it results in a dense matrix that lacks any block-diagonal structure or clear domain-based interpretation. Moreover, as described in Remark 4.1, in our approach, decomposing R_h leads to an algorithm in which it is only necessary to solve a PDE on a subgraph at each RBM step.
3. According to [31, Theorem 2], Theorem 2.2 still holds when we replace \mathbf{f}_h with a random counterpart $\mathbf{f}_{rb}(\omega)$ in the random system (2.6), provided that $\mathbb{E}[\mathbf{f}_{rb}] = \mathbf{f}_h$.

In [31], the Random Batch Method (RBM) was also adapted to address optimal control problems.

Specifically, let $Q, D \in \mathbb{R}^{N \times N}$ be two symmetric and positive definite matrices, and let $\mathbf{y}_d \in \mathbb{R}^N$ be a given target. Denote by $\|\mathbf{v}\|_Q^2 := \langle \mathbf{v}, Q\mathbf{v} \rangle$ and $\|\mathbf{v}\|_D^2 := \langle \mathbf{v}, D\mathbf{v} \rangle$ for $\mathbf{v} \in \mathbb{R}^N$, and consider the optimal control problem

$$\min_{\mathbf{f}_h \in L^2(0,T;\mathbb{R}^N)} \left\{ J_{D,Q}(\mathbf{f}_h) = \frac{1}{2} \int_0^T (\|\mathbf{f}_h(t)\|_D^2 + \|\mathbf{y}_h(t) - \mathbf{y}_d\|_Q^2) dt \right\}, \quad (2.13)$$

where \mathbf{y}_h is the solution of (2.6) with the right-hand side \mathbf{f}_h . A unique optimal pair $(\mathbf{y}_h, \mathbf{f}_h)$ solving (2.13) exists ([29, Section 1.4]).

Additionally, consider the ω -dependent optimal control problem

$$\min_{\mathbf{f}_R(\omega) \in L^2(0,T;\mathbb{R}^N)} \left\{ J_{D,Q}^R(\mathbf{f}_R(\omega)) = \frac{1}{2} \int_0^T (\|\mathbf{f}_R(t)\|_D^2 + \|\mathbf{y}_R(t) - \mathbf{y}_d\|_Q^2) dt \right\}, \quad (2.14)$$

where \mathbf{y}_R is the solution of the random dynamics (2.10) with the right-hand side given by $\mathbf{f}_R(\omega)$. For each realization of ω , a unique optimal pair $(\mathbf{y}_R(\omega), \mathbf{f}_R(\omega))$ exists.

From [31, Theorem 4], the following holds:

Theorem 2.3. *Let $(\mathbf{y}_h, \mathbf{f}_h)$ and $(\mathbf{y}_R, \mathbf{f}_R)$ denote the optimal pairs of the optimal control problems (2.13) and (2.14), respectively. Then, the following inequality holds:*

$$\mathbb{E}[\|\mathbf{f}_h(t) - \mathbf{f}_R(t)\|^2] + \mathbb{E}[\|\mathbf{y}_h(t) - \mathbf{y}_R(t)\|^2] \leq C_{oc}(1 + \|E_h^{-1}\|^2 T) \frac{\text{Var}[R_{rb}]}{\lambda_{\min}^2(D) \lambda_{\min}^2(E_h)} \delta, \quad (2.15)$$

for every $t \in (0, T)$, where $\lambda_{\min}(D)$ and $\lambda_{\min}(E_h)$ denotes the smaller eigenvalues of D and E_h respectively. The constant $C_{oc} > 0$ in (2.15) (whose subscript *oc* refers to “optimal control”) is given by

$$C_{oc} = 2\|D\|^2 ((1+T)(\|E_h^{-1}\mathbf{y}^0\| + \|E_h^{-1}\mathbf{f}_h\|)^2 + \|\mathbf{y}_d\|^2) \|E_h^{-1}\|^2 (\|E_h^{-1}R_h\|T^2 + 2T). \quad (2.16)$$

Here, the constant C_{oc} in (2.16) is obtained after carefully tracking the proofs in [31].

3. APPROXIMATION BY THE RANDOM BATCH METHOD

3.1. Approximation of the Heat Equation via the RBM. Let us consider the basis functions $\{\phi_j\}_{j=1}^N$ of the space V_h introduced in Section 2.1. Let $\mathbf{y}_R(\omega, t) \in \mathbb{R}^N$ be the solution of (2.10), and denote by

$$y_R(x, t, \omega) := \sum_{j=1}^N (\mathbf{y}_R)_j(\omega, t) \phi_j(x), \quad (3.1)$$

where $(\mathbf{y}_R)_j$ denotes the j -th coordinate of $\mathbf{y}_R(\boldsymbol{\omega}, t)$ on the basis of V_h .

In the following, to simplify the presentation, we assume that the matrices $\{R_{h,m}\}_{m=1}^M$ are such that $R_{h,m} = R_m/h$ for all $m \in \{1, \dots, M\}$, where each R_m is an $N \times N$ matrix whose entries are independent of h . This is the structure of the matrix R_h itself. In this setting, the following result holds:

Theorem 3.1. *Let y_R be as in (3.1) and let y be the solution of (2.1) with initial condition $y^0 \in H_0^1(0, L)$ and $f \in L^2(0, T; L^2(0, L))$. Then, for $h < \sqrt{6T}$ given, we have*

$$\mathbb{E}[\|y_R(t) - y(t)\|_{L^2(0,L)}^2] \leq C \left(h^4 + \frac{\delta}{h^7} C(M) \right), \quad (3.2)$$

for every $t \in (0, T)$, where C and $C(M)$ are two positive constants independent of h and δ , with $C(M)$ depending on the chosen decomposition and δ being the RBM parameter introduced in Section 2.2.

Remark 3.1. *To ensure the convergence of the error in (3.2), it is sufficient for δ to be small relative to h . In particular, taking $\delta = h^{7+\alpha}$, for some $\alpha > 0$, we deduce a convergence of order h^α . This is illustrated in Section 4.2.1.*

Proof. Given that $R_h = R/h$ and $R_{h,m} = R_m/h$ with R and R_m being $N \times N$ matrices with entries independent of h , we have

$$\text{Var}[R_{rb}] = \sum_{i=1}^{2^M} \left(\left\| R_h - \sum_{m \in S_i} \frac{R_{h,m}}{\pi_m} \right\|^2 p_i \right) \leq \frac{1}{h^2} \sum_{i=1}^{2^M} \left(\left\| R - \sum_{m \in S_i} \frac{R_m}{\pi_m} \right\|^2 p_i \right) = \frac{C(M)}{h^2}, \quad (3.3)$$

where the constant $C(M)$ is independent of h . On the other hand, since E_h is a tridiagonal Toeplitz matrix, its spectrum can be computed explicitly and, according to [19], its smallest eigenvalue is given by

$$\lambda_{\min}(E_h) = h \left(\frac{2}{3} + \frac{1}{3} \cos \left(\frac{N\pi}{N+1} \right) \right) > \frac{h}{3}. \quad (3.4)$$

Now observe that, since $(\mathbf{f}_h)_j = (f, \phi_j)_{L^2(0,L)}$, we have

$$\|\mathbf{f}_h\| = \left(\sum_{j=1}^N |(f, \phi_j)_{L^2(0,L)}|^2 \right)^{1/2} \leq \|f\|_{L^2(0,L)} \left(\sum_{j=1}^N \|\phi_j\|_{L^2(0,L)}^2 \right)^{1/2} \leq \|f\|_{L^2(0,L)} \left(\frac{2}{3} (L-h) \right)^{1/2}.$$

Here, we have used that $\|\phi_j\|_{L^2(0,L)}^2 = 2h/3$ for every $j \in \{1, \dots, N\}$ and that $Nh = L - h$. Since $h < L$ and $\|E_h^{-1}\| = 1/\lambda_{\min}(E_h)$, we obtain

$$\|E_h^{-1} \mathbf{f}_h\| \leq \frac{3L^{1/2} \|f\|_{L^2(0,L)}}{h}, \quad (3.5)$$

and, similarly,

$$\|E_h^{-1} \mathbf{y}_h^0\| \leq \frac{3L^{1/2} \|y^0\|_{L^2(0,L)}}{h}. \quad (3.6)$$

Moreover, since $\|R_h\| \leq 4/h$ and $h < \sqrt{6T}$, we obtain

$$(\|E_h^{-1} R_h\| T^2 + 2T) \leq \frac{24T^2}{h^2}. \quad (3.7)$$

Estimate (3.2) can now be established with the aid of y_h , solution of (2.5). Applying Theorem 2.1, we deduce that

$$\begin{aligned} \|y_R(t, \boldsymbol{\omega}) - y(t)\|_{L^2(0,L)}^2 &\leq 2 \left(\|y_R(t, \boldsymbol{\omega}) - y_h(t)\|_{L^2(0,L)}^2 + \|y_h(t) - y(t)\|_{L^2(0,L)}^2 \right) \\ &\leq \frac{4h}{3} \|\mathbf{y}_R(t, \boldsymbol{\omega}) - \mathbf{y}_h(t)\|^2 + Ch^4. \end{aligned} \quad (3.8)$$

Taking the expectation in (3.8), applying Theorem 2.2 and estimates (3.3), (3.4), (3.5), (3.6), and (3.7) the proof is concluded. \square

Remark 3.2. *Several remarks are in order:*

1. *The factor h^7 dividing in (3.2) arises due to the fact that the right-hand side of (2.12) depends on the l^2 -norm of the matrices R_h and E_h^{-1} , and $1/\lambda_{\min}(E_h)$, where each is of the order $1/h$. Also $\text{Var}[R_{rb}]$ depends on $1/h^2$. This leads us to the dividing factor h^7 .*

2. Note that when h approaches zero, the discretized PDE becomes closer to the original PDE; however, if δ is fixed and h decreases, the RBM departs from the discretized PDE since the size of the problem increases. The condition $\delta = O(h^7)$ is needed to ensure that the RBM remains close to the discretized PDE and, therefore, to the original PDE when h approaches zero.
3. The multiplicative constant $C(M)$ in (3.3) plays a relevant role in the error estimate (3.2), since it amplifies the error term δ/h^7 . Consequently, minimizing $C(M)$ is a relevant objective in our setting, as it directly impacts the overall efficiency of the method. Moreover, the value of $C(M)$ is closely linked to the way the matrix R_h is decomposed – an aspect we further elaborate on in Section 5. In particular, when $M = 1$, the RBM reduces to the standard FEM approximation, and in this case we have $C(M) = 0$.
4. By Theorem 3.1 we have that the variance

$$\mathbb{V}[\|y_R(t) - y(t)\|] := \mathbb{E}[\|y_R(t) - y(t)\|^2] - (\mathbb{E}[\|y_R(t) - y(t)\|])^2 \leq C \left(h^4 + \frac{\delta}{h^7} C(M) \right).$$

Moreover, Markov's inequality yields, for any $\varepsilon > 0$,

$$\mathbb{P}(\|y_R(t) - y(t)\|^2 > \varepsilon) \leq \frac{C}{\varepsilon} \left(h^4 + \frac{\delta}{h^7} C(M) \right).$$

Therefore, whenever $C(h^4 + \delta/h^7 C(M))$ is small, not only the mean-square error but also the variance and the probability of large deviations are uniformly small. In this regime, a single realization of the scheme suffices to approximate the expected error with high probability.

5. The analysis in Theorems 3.1 and 3.2 (below) can be adapted and applied to the finite difference method (FDM). However, obtaining estimates similar to (2.4) with the FDM, requires smoother data to ensure that $y \in L^2(0, T; C^4(0, L))$ (see, for instance, [12, Theorem 16.5], where the convergence error for the FDM depends on $\|\partial_x^4 y\|_{L^2(0, T; C(0, L))}$).

3.2. Application to Optimal Control. In this section, we prove the convergence of the RBM in the context of optimal control for the heat equation; we employ a discrete approach. Namely, we first discretize the PDE to later apply the RBM. Let $y_d \in H_0^1(0, L)$ be a given target, and consider the optimal control problem

$$\min_{f \in L^2(0, T; L^2(0, L))} \left\{ J(f) = \frac{1}{2} \int_0^T \left(\|f(t)\|_{L^2(0, L)}^2 + \|y(t) - y_d\|_{L^2(0, L)}^2 \right) dt \right\}, \quad (3.9)$$

where y is the solution of (2.1) with right-hand side f . According to [29, Chapter 3], there exists a unique optimal pair (y, f) for (3.9). To approximate the optimal control problem (3.9), we can consider the finite-dimensional problem

$$\min_{f_h \in L^2(0, T; L^2(0, L))} \left\{ J_h(f_h) = \int_0^T \left(\|f_h(t)\|_{L^2(0, L)}^2 + \|y_h(t) - y_d\|_{L^2(0, L)}^2 \right) dt \right\}, \quad (3.10)$$

where y_h is the solution of (2.3) with right-hand side f_h . The convergence of the FEM in this context, is assured by the following result in [18].

Theorem 3.2. *Let (y, f) denote the optimal pair of (3.9) with $y^0, y_d \in H_0^1(0, L)$, and let (y_h, f_h) denote the optimal pair of (3.10). Then, there exists a constant $C > 0$, independent of $h > 0$, such that*

$$\|y_h(t) - y(t)\|_{L^2(0, L)}^2 + \|f_h(t) - f(t)\|_{L^2(0, L)}^2 \leq Ch^4 \left(\frac{T}{t(T-t)} + \ln \left(\frac{1}{h} \right) \right)^2,$$

for every $t \in (0, T)$.

Denote by $(\mathbf{y}_h, \mathbf{f}_h)$ the vectors of coefficients of (y_h, f_h) . Observe that

$$\|y_h(t)\|_{L^2(0, L)}^2 = \left\| \sum_{j=1}^N y_j(t) \phi_j \right\|_{L^2(0, L)}^2 = \|\mathbf{y}_h\|_{E_h}^2 = \langle E_h \mathbf{y}_h, \mathbf{y}_h \rangle, \quad (3.11)$$

where E_h corresponds to the mass matrix introduced in (2.7). Therefore, when $D = Q = E_h$, then $(\mathbf{y}_h, \mathbf{f}_h)$ corresponds to the optimal pair of the finite-dimensional problem (2.13) restricted to the system (2.6), with \mathbf{y}_d taken as the vector of coefficients of the projection of y_d onto V_h .

Let us denote by $(\mathbf{y}_R, \mathbf{f}_R)$ the optimal pair of the random optimal control problem (2.14) restricted to (2.10), and denote by (y_R, f_R) its projection onto V_h . Then, we have the following theorem.

Theorem 3.3. *Let (y, f) denote the optimal pair of (3.9) with $y^0, y_d \in H_0^1(0, L)$, and let (y_R, f_R) be as given above. Then, there exists a constant $C > 0$, independent of h and δ , such that*

$$\mathbb{E} \left[\|y_R(t) - y(t)\|_{L^2(0,L)}^2 \right] + \mathbb{E} \left[\|f_R(t) - f(t)\|_{L^2(0,L)}^2 \right] \leq C \left(\frac{\delta}{h^{11}} C(M) + h^4 \left(\frac{T}{t(T-t)} + \ln \left(\frac{1}{h} \right) \right)^2 \right), \quad (3.12)$$

for every $t \in (0, T)$, where $C(M)$ is the same constant as in Theorem 3.1.

Proof. Applying Theorem 3.2 and using the fact that $\|\phi_j\|_{L^2(0,L)}^2 = 2h/3$, we obtain

$$\begin{aligned} \mathbb{E} \left[\|y_R(t) - y(t)\|_{L^2(0,L)}^2 \right] &\leq \mathbb{E} \left[\|y_R(t) - y_h(t)\|_{L^2(0,L)}^2 \right] + \mathbb{E} \left[\|y_h(t) - y(t)\|_{L^2(0,L)}^2 \right] \\ &\leq \mathbb{E} \left[\sum_{j=1}^N \|(\mathbf{y}_R)_j(t) - (\mathbf{y}_h)_j(t)\|^2 \right] \|\phi_j\|_{L^2(0,L)}^2 + Ch^4 \left(\frac{T}{t(T-t)} + \ln \left(\frac{1}{h} \right) \right)^2 \\ &\leq \mathbb{E} [\|\mathbf{y}_R(t) - \mathbf{y}_h(t)\|^2] \frac{3h}{2} + Ch^4 \left(\frac{T}{t(T-t)} + \ln \left(\frac{1}{h} \right) \right)^2. \end{aligned}$$

To estimate the first term on the right-hand side, we will use Theorem 2.3. Recall that $D = E_h$, $\|E_h^{-1}\| = 1/\lambda_{\min}(E_h)$, and the estimations (3.4), (3.5), and (3.6). Then, we deduce that the constant C_{oc} from (2.16) is bounded by

$$C_{oc} \leq Ch^2 \left((1+T) \left(\frac{1}{h^2} + \frac{1}{h^2} + 1 \right) \frac{1}{h^2} \left(\frac{T^2}{h^2} + 2T \right) \right) \leq \frac{C_1}{h^4}, \quad (3.13)$$

where C_1 is independent of h and the decomposition of R_h . Analogous to (3.3), we have that

$$(1 + \|E_h^{-1}\|^2 T) \frac{\text{Var}[R_{rb}]}{\lambda_{\min}^4(E_h)} \leq \frac{C(M)}{h^8}, \quad (3.14)$$

where $C(M)$ is defined as in (3.3). Then, by combining Theorem 2.3 with the estimates (3.13) and (3.14), we deduce (3.12)

$$\mathbb{E} [\|\mathbf{y}_h(t) - \mathbf{y}_R(t)\|^2] \frac{3h}{2} \leq C_{oc} (1 + \|E_h^{-1}\|^2 T) \frac{\text{Var}[R_{rb}]}{\lambda_{\min}^4(E_h)} \delta \leq \frac{C_1 C(M) \delta}{h^{11}}. \quad (3.15)$$

Performing an analogous computation for the expectation of the differences in the optimal controls yields the same upper bound. \square

Remark 3.3. *Note the following:*

1. Whereas Theorem 3.1 yields a denominator of order h^7 , Theorem 3.3 leads to a higher-order term of h^{11} . This additional factor originates from Theorem 2.3, which – unlike (2.12) – introduces extra constants of order h^{-1} . When these contributions are propagated through the estimates in (3.13) and (3.14), they accumulate, resulting in the overall h^{11} dependence in the denominator, as demonstrated in (3.15).
2. Similar to Remark 3.2, by taking $\delta = h^{11+\varepsilon}$, we guarantee a convergence rate h^ε .
3. The logarithmic factor in Theorem 3.3 arises from our reliance on Theorem 3.2 (originally from [18]) as an intermediate estimate. In that result, the authors show that the semigroup error satisfies

$$\|\mathcal{T}(t) - \mathcal{T}_h(t)P_h\|_{\mathcal{L}(L^2(0,1))} \leq c_1 e^{c_2(t-s)} (t-s)^{-1}, \quad 0 \leq s < t \leq T, \quad (3.16)$$

where $\mathcal{T}(t)$ and $\mathcal{T}_h(t)$ denote the infinite- and finite-dimensional semigroups, respectively, P_h is the orthogonal projection, and $c_1, c_2 > 0$ are constants.

To bound the error in the optimal state, Duhamel's formula is applied. When the resulting time integral is split appropriately, the singularity in the integrand – represented by the factor $(t-s)^{-1}$ – gives rise to a logarithmic contribution, namely $-\ln(h) = \ln(1/h)$. This term then propagates to the final error estimate for the optimal control.

We remark that even in more recent and generalized results (see [1] and references therein), the same logarithmic factor $\ln(1/h)$ persists.

4. THE RBM FOR THE HEAT EQUATION ON NETWORKS

In this section, we present the heat equation on graphs and discuss its discretization and the application of the RBM.

4.1. The Heat Equation on Graphs. Let $\mathcal{G} := (\mathcal{E}, \mathcal{V})$ be an oriented and connected metric graph with vertices $v \in \mathcal{V}$ and edges $e \in \mathcal{E}$. In the following, to simplify the presentation, we will focus on the graph \mathcal{G} illustrated in Figure 1. Nonetheless, the methodology developed herein is applicable to any connected metric graph. The graph \mathcal{G} is composed by the edges and vertices:

$$\mathcal{E} = \{e_i\}_{i=1}^{10}, \quad \text{and} \quad \mathcal{V} = \mathcal{V}_0 \cup \mathcal{V}_b = \{v_i\}_{i=1}^3 \cup \{v_i\}_{i=4}^{11},$$

where \mathcal{V}_0 and \mathcal{V}_b denote the interior and boundary vertices, respectively. Here, the orientation of the graph is used merely to identify each edge $e \in \mathcal{E}$ with an interval $(0, l_e)$ for $l_e > 0$, without ambiguity, where 0 and l_e represent the incoming and outgoing vertices of e , respectively. For simplicity, we also assume that $l_e = L > 0$ for all $e \in \mathcal{E}$.

On each edge e_i with $i \in \{1, \dots, 10\}$, we consider the heat equation

$$\begin{cases} \partial_t y^{e_i} - \partial_{xx} y^{e_i} = f^{e_i}, & (x, t) \in (0, L) \times (0, T), \\ y^{e_i}(x, 0) = y_{e_i}^0(x), & x \in (0, L), \end{cases} \quad (4.1)$$

where $y_{e_i}^0$ is the initial condition and f^{e_i} is the source term, both defined for every $i \in \{1, \dots, 10\}$. System (4.1) is complemented with boundary and coupling conditions:

$$\begin{cases} y^e(v, t) = 0, & v \in \mathcal{V}_b, e \in \mathcal{E}(v), \\ y^{e'}(v, t) = y^{e''}(v, t), & v \in \mathcal{V}_0, e', e'' \in \mathcal{E}(v), \\ \sum_{e \in \mathcal{E}(v)} \partial_x y^e(v, t) n_e(v) = 0, & v \in \mathcal{V}_0, \end{cases} \quad (4.2)$$

over the time interval $(0, T)$. Here, $n_e(v)$ denotes the incidence vector of the directed graph, and $\mathcal{E}(v)$ denotes the set of edges incident to the vertex v . The first equation in (4.2) corresponds to a natural extension of the null Dirichlet boundary condition. The second and third conditions of (4.2) are coupling conditions for the interior vertices of the graph. In the following, we denote by f and y^0 the sets of functions $\{f^{e_i}\}_{i=1}^{10}$ and $\{y_{e_i}^0\}_{i=1}^{10}$, respectively. We assume that $f \in L^2(0, T; L^2(\mathcal{E}))$ and $y^0 \in H_0^1(\mathcal{E})$ (see [23, Chapter 3] for an introduction to Lebesgue and Sobolev spaces on graphs). The well-posedness of the system (4.1)-(4.2) has been studied in [6], ensuring the existence of a unique solution $y \in C(0, T; L^2(\mathcal{E})) \cap L^2(0, T; H_0^1(\mathcal{E}))$.

In the following, we consider the initial condition y^0 and the source term f as specified in Table 1. The exact solution of (4.1)-(4.2), associated with this data, is also given in Table 1. The sequence of coefficients $\{p_{e_i}\}_{i=1}^{10}$, defined in Table 2, is carefully chosen so that y^e satisfies (4.1)-(4.2) with the corresponding data. This construction follows the method of manufactured solutions, as described in [2, Chapter 12]. That is, we begin by prescribing a smooth candidate function y^e as the exact solution and then define f and y^0 accordingly, ensuring that the equation and boundary conditions are satisfied. This approach allows for a controlled setting in which the numerical error can be precisely assessed.

TABLE 1. Expressions for $y_{e_i}^0(x)$, $f^{e_i}(x, t)$ and $y^{e_i}(x, t)$ for $i \in \{1, \dots, 10\}$.

$y_{e_i}^0(x)$	$f^{e_i}(x, t)$	$y^{e_i}(x, t)$
$p_{e_i} \cdot x \cdot (1 - x)$	$p_{e_i} \cdot (2 - x + x^2) \cdot e^{-t}$	$p_{e_i} \cdot x \cdot (1 - x) \cdot e^{-t}$

TABLE 2. Coefficients p_{e_i} for $i \in \{1, \dots, 10\}$ used to introduce the problem data.

p_{e_1}	p_{e_2}	p_{e_3}	p_{e_4}	p_{e_5}	p_{e_6}	p_{e_7}	p_{e_8}	p_{e_9}	$p_{e_{10}}$
1	-1	-1	1	-1	-1	-1	2	-1	-1

We will use finite elements to introduce a semi-discrete version of the system (4.1)-(4.2). For this purpose, it is necessary to introduce a finite-dimensional space $V_h^\mathcal{E}$ to approximate $H_0^1(\mathcal{E})$. On each edge e_i for $i \in \{1, \dots, 10\}$, we introduce the spatial mesh $\{x_j^i\}_{j=0}^{N+1}$ with step size h . Due to the structure of the graph, we identify the vertices as follows:

$$x_{N+1}^1 = x_0^2 = x_0^3 = x_0^4, \quad x_{N+1}^4 = x_0^5 = x_0^6 = x_0^7 = x_{N+1}^8, \quad x_{N+1}^9 = x_0^8 = x_0^{10}.$$

On each edge e_i we can introduce the basis functions $\{\phi_j^i\}_{j=1}^N$ as in Section 2.1. These functions span a finite-dimensional space that can be used to approximate the solution in the interior of each edge. However, we also need to introduce basis functions to approximate the solution on the graph's interior vertices, or junctions. For this, we define the functions $\{\phi_0^4, \phi_0^6, \phi_0^{10}\}$ as follows:

$$\phi_0^4(x) = \begin{cases} (x - x_N^1)/h, & \text{if } x \in [x_N^1, x_0^4], \\ (x_1^2 - x)/h, & \text{if } x \in [x_0^4, x_1^2], \\ (x_1^3 - x)/h, & \text{if } x \in [x_0^4, x_1^3], \\ (x_1^4 - x)/h, & \text{if } x \in [x_0^4, x_1^4], \end{cases} \quad \phi_0^6(x) = \begin{cases} (x - x_N^4)/h, & \text{if } x \in [x_N^4, x_0^6], \\ (x_1^5 - x)/h, & \text{if } x \in [x_0^6, x_1^5], \\ (x_1^6 - x)/h, & \text{if } x \in [x_0^6, x_1^6], \\ (x_1^7 - x)/h, & \text{if } x \in [x_0^6, x_1^7], \\ (x - x_N^8)/h, & \text{if } x \in [x_N^8, x_0^6], \end{cases}$$

$$\phi_0^{10}(x) = \begin{cases} (x - x_N^9)/h, & \text{if } x \in [x_N^9, x_0^{10}], \\ (x_1^8 - x)/h, & \text{if } x \in [x_0^{10}, x_1^8], \\ (x_1^{10} - x)/h, & \text{if } x \in [x_0^{10}, x_1^{10}], \end{cases}$$

vanishing away from their domain of definition. The basis functions ϕ_0^4 and ϕ_0^6 are illustrated in Figure 2.

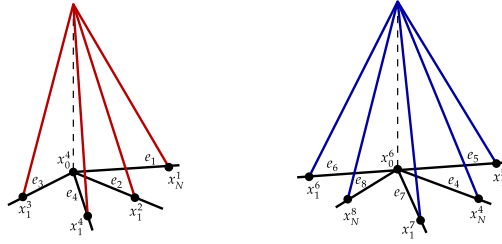


FIGURE 2. Illustration of the basis functions defined at the interior vertices x_0^4 and x_0^6 of the graph. Both functions attain a maximum value of 1.

Let us consider the space $V_h^\mathcal{E}$ as the span of the functions $\{\phi_0^4, \phi_0^6, \phi_0^{10}\} \cup \bigcup_{i=1}^{10} \bigcup_{j=1}^N \{\phi_j^i\}$. Observe that the finite-dimensional space $V_h^\mathcal{E}$ is a natural finite element approximation of the space $H_0^1(\mathcal{E})$. Let us assume that $y^0 \in H_0^1(\mathcal{E})$, and denote by y_h^0 the projection of y^0 onto $V_h^\mathcal{E}$ with respect to the scalar product in $H_0^1(\mathcal{E})$. Then, we can introduce a weak formulation of the system (4.1)-(4.2) as follows: Find $y_h \in C^1(0, T; V_h^\mathcal{E})$ such that

$$\begin{cases} \sum_{i=1}^{10} \left(\int_0^L \partial_t y_h^{e_i}(x, t) \phi_j^i(x) + \partial_x y_h^{e_i}(x, t) \partial_x \phi_j^i(x) dx \right) = \sum_{i=1}^{10} \int_0^L f^{e_i}(x, t) \phi_j^i(x) dx, \\ \int_0^L y_h^{e_i}(x, 0) \phi_j^i(x) = \int_0^L y_{h, e_i}^0(x) \phi_j^i(x) dx, \end{cases} \quad (4.3)$$

for every $t \in (0, T)$. The solution on each edge $y_h^{e_i}$ can be written as

$$y_h^{e_i}(x, t) = \begin{cases} \sum_{j=0}^N y_j^{e_i}(t) \phi_j^i(x), & \text{if } i \in \{4, 6, 10\}, \\ \sum_{j=1}^N y_j^{e_i}(t) \phi_j^i(x), & \text{otherwise.} \end{cases} \quad (4.4)$$

Observe that we have adopted the convention of storing the coefficient value of the solution associated with the interior vertices on the edges e_4 , e_6 , and e_{10} . Therefore, the representation of the solution as

a linear combination of the basis elements for these edges begins with index 0 (i.e., includes one extra coefficient).

Then, let us consider the vector of coefficients $\mathbf{Y}_h(t) = (\mathbf{y}_h^{e_1}(t), \dots, \mathbf{y}_h^{e_{10}}(t))^\top$, where

$$\begin{cases} \mathbf{y}_h^{e_i} = (y_0^{e_i}(t), \dots, y_N^{e_i}(t))^\top, & \text{if } i \in \{4, 6, 10\}, \\ \mathbf{y}_h^{e_i} = (y_1^{e_i}(t), \dots, y_N^{e_i}(t))^\top, & \text{otherwise.} \end{cases} \quad (4.5)$$

Here, $\mathbf{Y}_h(t) \in \mathbb{R}^{10N+3}$ (with N discretization points for each of the 10 edges and 3 extra discretization points for the internal vertices). We also introduce the vectors $\mathbf{F}_h(t) = (\mathbf{f}_h^{e_1}, \dots, \mathbf{f}_h^{e_{10}})$, where

$$\begin{cases} \mathbf{f}_h^{e_i} = (f_0^{e_i}(t), \dots, f_N^{e_i}(t))^\top, & \text{if } i \in \{4, 6, 10\}, \\ \mathbf{f}_h^{e_i} = (f_1^{e_i}(t), \dots, f_N^{e_i}(t))^\top, & \text{otherwise,} \end{cases}$$

with $f_j^{e_i} = (f^{e_i}, \phi_j)_{L^2(0,L)}$. Similarly to (4.4) and (4.5), we introduce $\mathbf{Y}_h^0 = (\mathbf{y}_{0,h}^{e_1}, \dots, \mathbf{y}_{0,h}^{e_{10}})$. Observe that \mathbf{Y}_h satisfies the following system:

$$\begin{cases} \mathbf{E}_h \partial_t \mathbf{Y}_h + \mathbf{R}_h \mathbf{Y}_h = \mathbf{F}_h, & t \in (0, 1), \\ \mathbf{E}_h \mathbf{Y}_h(0) = \mathbf{Y}_h^0. \end{cases} \quad (4.6)$$

The matrix \mathbf{R}_h is given by

$$\mathbf{R}_h = \begin{bmatrix} e_1 & e_2 & e_3 & v_1 & e_4 & e_5 & v_2 & e_6 & e_7 & e_8 & e_9 & v_3 & e_{10} \end{bmatrix} \quad (4.7)$$

$$\left(\begin{array}{c|c|c|c|c|c|c|c|c|c|c|c|c} \mathbf{R}_h^1 & c_1^4 & 0 & 0 & 0 & 0 & 0 & 0 & 0 & 0 & 0 & 0 \\ \hline a_1^4 & a_2^4 & a_3^4 & \frac{4}{h} & a_4^4 & 0 & 0 & 0 & 0 & 0 & 0 & 0 \\ \hline 0 & c_2^4 & \mathbf{R}_h^2 & c_1^6 & 0 & 0 & 0 & 0 & 0 & 0 & 0 & 0 \\ \hline 0 & 0 & a_4^6 & a_5^6 & \frac{5}{h} & a_6^6 & a_7^6 & a_8^6 & 0 & 0 & 0 & 0 \\ \hline 0 & 0 & 0 & c_2^6 & \mathbf{R}_h^3 & c_1^{10} & 0 & 0 & 0 & 0 & 0 & 0 \\ \hline 0 & 0 & 0 & 0 & 0 & 0 & 0 & a_8^{10} & a_9^{10} & \frac{3}{h} & a_{10}^{10} & 0 \\ \hline 0 & 0 & 0 & 0 & 0 & 0 & 0 & 0 & 0 & c_2^3 & R_h & 0 \end{array} \right), \quad (4.8)$$

where $\mathbf{R}_h^1 = \text{Diag}(R_h, R_h, R_h)$, $\mathbf{R}_h^2 = \text{Diag}(R_h, R_h)$, and $\mathbf{R}_h^3 = \text{Diag}(R_h, R_h, R_h, R_h)$ are block diagonal matrices, with $R_h \in \mathbb{R}^{N \times N}$ being the stiffness matrix introduced in (2.7). For each $k \in \{4, 6, 10\}$, the vectors $a_i^k \in \mathbb{R}^N$ have coordinates $(\partial_x \phi_j^k, \partial_x \phi_0^i)_{L^2(0,L)}$ for $j \in \{1, \dots, N\}$. The values of these vectors correspond to the inner products between the basis elements and the functions at the interior vertices. Finally, observe that the column vectors c_i^k are such that the matrix \mathbf{R}_h is symmetric, i.e., $c_1^4 = (a_1^4, a_2^4, a_3^4)^\top$, $c_2^4 = (a_4^4, 0)^\top$, and so on. The symmetry of \mathbf{R}_h arises from the symmetry of the product $(\partial_x \phi_j^k, \partial_x \phi_n^i)_{L^2(0,L)}$ for $j, n \in \{1, \dots, N\}$.

The vector, within square brackets, above the matrix \mathbf{R}_h , indicates which sector of the graph each block corresponds to (for example, \mathbf{R}_h^1 represents the discretization of the dynamics on edges e_1, e_2 , and e_3).

Similarly, \mathbf{E}_h is a symmetric and positive definite matrix sharing the same structure as (4.7), where the block diagonal matrices are defined using the mass matrix E_h from (2.7).

It is worth noting that \mathbf{R}_h not only encodes information about the dynamics but also incorporates the topological structure of the graph, including the coupling conditions at the interior vertices. The decomposition of \mathbf{R}_h will be performed taking into account the structure of the graph. In the next section, we present two examples of decompositions: one with *overlapping* and one *without overlapping* (non-overlapping).

4.2. Numerical Simulations. In this section, we aim to corroborate Theorem 3.1 and Theorem 3.3. We begin with an overlapping decomposition example and subsequently discuss a non-overlapping one. Most of our analysis is developed for the overlapping case, as the non-overlapping decomposition is completely analogous. In the overlapping decomposition case, we verify Remark 3.2 to illustrate convergence, and we also compare the computational time and memory usage of the RBM.

Computational Setup. All numerical experiments were executed on a device featuring an AMD Ryzen 9 5900HS processor with Radeon Graphics, clocked at 3.30 GHz, and equipped with 16.0 GB of RAM (with 15.4 GB usable). The experiments were implemented in Python, utilizing the NumPy and SciPy libraries.

4.2.1. *Overlapping decomposition.* Let us introduce the following decomposition of the matrix \mathbf{R}_h :

$$\mathbf{R}_h = \begin{pmatrix} \mathbf{B}_1 & 0 & 0 \\ 0 & 0 & 0 \\ 0 & 0 & 0 \end{pmatrix} + \begin{pmatrix} 0 & 0 & 0 \\ 0 & \mathbf{B}_2 & 0 \\ 0 & 0 & 0 \end{pmatrix} + \begin{pmatrix} 0 & 0 & 0 \\ 0 & 0 & 0 \\ 0 & 0 & \mathbf{B}_3 \end{pmatrix} = \mathbf{R}_1 + \mathbf{R}_2 + \mathbf{R}_3, \quad (4.9)$$

where the matrices $\mathbf{B}_1 \in \mathbb{R}^{N_1 \times N_1}$, $\mathbf{B}_2 \in \mathbb{R}^{N_2 \times N_2}$, and $\mathbf{B}_3 \in \mathbb{R}^{N_3 \times N_3}$ are given by

$$\mathbf{B}_1 = \begin{pmatrix} \mathbf{R}_h^1 & c_1^1 & 0 \\ a_1^1 & a_2^1 & a_3^1 & 4/h & a_4^1 \\ 0 & c_2^1 & \frac{R_h}{2} \end{pmatrix}, \quad \mathbf{B}_2 = \begin{pmatrix} \frac{R_h}{2} & 0 & c_1^2 & 0 & 0 \\ 0 & R_h & c_2^2 & 0 & 0 \\ a_4^2 & a_5^2 & 5/h & a_6^2 & a_7^2 & a_8^2 \\ 0 & 0 & c_3^2 & \mathbf{R}_h^2 & 0 \\ 0 & 0 & 0 & 0 & \frac{R_h}{2} \end{pmatrix}, \quad \mathbf{B}_3 = \begin{pmatrix} \frac{R_h}{2} & 0 & c_1^3 & 0 \\ 0 & R_h & c_2^3 & 0 \\ 0 & a_8^3 & a_9^3 & 3/h & a_{10}^3 \\ 0 & 0 & c_3^3 & R_h \end{pmatrix}, \quad (4.10)$$

where $N_1 = 4N + 1$, $N_2 = 5N + 1$ and $N_3 = 3N + 1$. The matrices \mathbf{B}_1 and \mathbf{B}_2 were constructed to share the last and first block matrix, respectively, associated with edge e_4 . Similarly, \mathbf{B}_2 and \mathbf{B}_3 share their last and first block matrix, associated with edge e_8 . This decomposition can be interpreted as an *overlapping decomposition*, where the matrices \mathbf{B}_1 , \mathbf{B}_2 , and \mathbf{B}_3 represent the dynamics on the edges adjacent to vertices v_1 , v_2 , and v_3 , respectively. This is illustrated in Figure 1, where the dynamics on the subgraph with edges $\{e_1, e_2, e_3, e_4\}$ is driven by matrix \mathbf{B}_1 . Similarly, the dynamics on the subgraphs with edges $\{e_4, e_5, e_6, e_7, e_8\}$ and $\{e_8, e_9, e_{10}\}$ are driven by the matrices \mathbf{B}_2 and \mathbf{B}_3 , respectively.

To introduce the random system, we consider the subsets S_i of $\{1, 2, 3\}$ (since $M = 3$). Let us decompose \mathbf{F}_h as

$$\mathbf{F}_h = (\mathbf{F}_1, 0, 0)^\top + (0, \mathbf{F}_2, 0)^\top + (0, 0, \mathbf{F}_3)^\top,$$

where

$$\mathbf{F}_1 = \left(\mathbf{f}_h^{e_1}, \mathbf{f}_h^{e_2}, \mathbf{f}_h^{e_3}, \frac{\mathbf{f}_h^{e_4}}{2} \right)^\top, \quad \mathbf{F}_2 = \left(\frac{\mathbf{f}_h^{e_4}}{2}, \mathbf{f}_h^{e_5}, \mathbf{f}_h^{e_6}, \mathbf{f}_h^{e_7}, \frac{\mathbf{f}_h^{e_8}}{2} \right)^\top, \quad \mathbf{F}_3 = \left(\frac{\mathbf{f}_h^{e_8}}{2}, \mathbf{f}_h^{e_9}, \mathbf{f}_h^{e_{10}} \right)^\top.$$

We define

$$S_1 = \{1\}, \quad S_2 = \{2\}, \quad S_3 = \{3\}, \quad \text{and} \quad p_1 = p_2 = p_3 = 1/3,$$

and $p_i = 0$ for remainder $i \in \{1, \dots, 8\} \setminus \{1, 2, 3\}$. Thus we have that $\pi_1 = \pi_2 = \pi_3 = 1/3$. Now, we can introduce a matrix \mathbf{R}_{rb} as in (2.9). Within this setting, at each time interval, \mathbf{R}_{rb} is assigned a randomly chosen matrix \mathbf{R}_i with probability $1/3$. Then, define \mathbf{Y}_R as the solution of the equation

$$\begin{cases} \mathbf{E}_h \partial_t \mathbf{Y}_R + \mathbf{R}_{rb} \mathbf{Y}_R = \mathbf{F}_{rb}, & t \in (0, T), \\ \mathbf{E}_h \mathbf{Y}_R(0) = \mathbf{Y}_h^0. \end{cases} \quad (4.11)$$

Here, following Remark 2.2, the function \mathbf{F}_{rb} is defined by

$$\mathbf{F}_{rb}(t) = \sum_{m \in S_{\omega_k}} \frac{\mathbf{F}_m}{\pi_m}, \quad t \in [(k-1)\delta, k\delta), \quad (4.12)$$

for each $k \in \{1, \dots, K\}$. Similar to \mathbf{R}_{rb} , the function \mathbf{F}_{rb} also satisfies $\mathbb{E}[\mathbf{F}_{rb}] = \mathbf{F}_h$.

For the spatial discretization, we use $N = 300$ elements on each edge, and therefore $\mathbf{R}_{rb} \in \mathbb{R}^{3003 \times 3003}$. In the following, we take $T = L = 1$ for simplicity. We compute the numerical solution of system (2.10) using an implicit Euler discretization (IE) with a uniform time step $\Delta t = T/(\zeta - 1)$, where $\zeta = 201$ is the number of time collocation points. To compute the expectation of \mathbf{Y}_R , we perform 30 realizations and then average them. It is worth noting that each realization can be computed independently, allowing for parallel execution and thus not increasing the overall computational time.

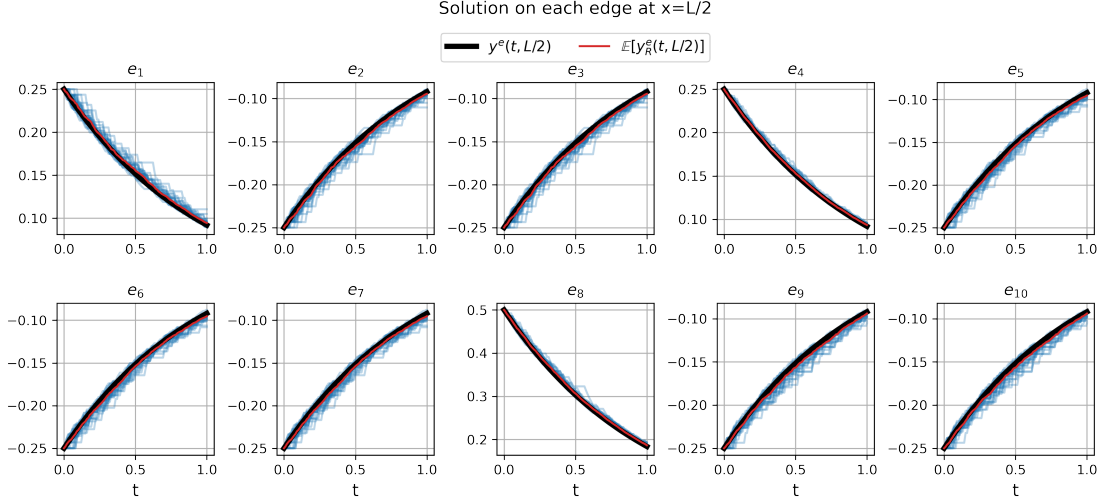


FIGURE 3. Comparison between the exact solution (in black) and the approximate solution (in red) at $x = L/2$ for each edge, using the RBM with the *overlapping* decomposition. The blue lines denote the different realizations.

To evaluate the performance of the discretize+RBM scheme, we set the parameter $\delta = 2\Delta t = 0.01$. Note that, with this choice, convergence cannot be inferred from Theorem 3.1 since $\delta \neq h^7$. Nevertheless, as we shall show, these parameters yield satisfactory accuracy relative to the full-network solution. Moreover, we observe that almost all realizations remain close to the average.

The numerical results displayed in Figure 3 indicate that the expected value of the solution of the random system is close to the exact solution, with small variance; individual realizations exhibit no significant deviation from the average. Table 3 shows the error of the full-graph and the exact solution (given by Table 1), and the (average) error between the *discretize+RBM* and the exact solution. Additionally, Table 3 compares the (average) memory usage and execution time between solving *discretize+RBM* and the entire graph problem directly with the implicit Euler scheme. Here, the (average) memory usage is computed by first analyzing the peak memory usage of each realization and then averaging all the memory usage picks. The execution time is computed by averaging the execution time of each realization. The results indicate that the RBM-based approach uses half as much memory and is twice as fast as the full-graph solution. This trade-off involves a slight reduction in solution resolution, yet the error remains comparable, and the discretize+RBM method achieves twice the speed of the full-graph approach.

TABLE 3. Comparison of the (average) maximum memory usage, error, and (average) execution time between the discretize+RBM approach and the full-graph implicit Euler method. The error is computed using the L^∞ -norm in time and L^2 -norm in space for the full-graph method, and the L^∞ -norm in time and expected L^2 -norm in space for the discretize+RBM scheme.

Method	Memory usage (MB)	Error	Execution time (s)
Discretize+RBM	187.88	9.3951e-03	2.72
Full-Graph	418.52	9.6152e-03	6.78

Following Remark 3.2, to corroborate Theorem 3.1, we consider different values for h . For $\varepsilon > 0$, we choose $\delta = h^{7/(1-\varepsilon)}$. With this choice, the error in Theorem 3.1 decreases at a rate of at least δ^ε . By selecting $\varepsilon = 10^{-4}$, we obtain the results shown in Figure 4, which illustrates the convergence. Observe that the convergence rate is approximately $\delta^{0.2}$, which is faster than the expected rate of δ^ε .

Table 4 presents the error values and the corresponding h values. Here, *Error RBM* denotes the L^∞ -norm in time and expected L^2 -norm in space between the exact solution and the Discretize+RBM

approach. Conversely, *Error Full-Graph* represents the L^∞ -norm in time and L^2 -norm in space between the exact solution and the solution computed on the full graph. Since $\delta = o(h^7)$ and $\Delta t \leq \delta$, we have chosen small h values to validate our results. The *Speedup* column corresponds to the quotient between the computational time of *Full-Graph* and *Discretize+RBM*. As h decreases, the discretize+RBM scheme not only speeds up computational time but may also deliver higher accuracy. However, this trend does not necessarily hold for smaller h , as observed, for instance, in Table 3, where at $h = 0.003$ the RBM accuracy, while still close, falls slightly below that of the full-graph solution.

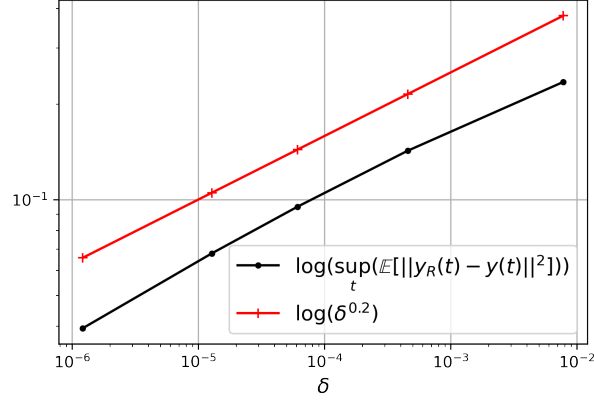


FIGURE 4. This figure illustrates the algorithm's convergence as $\delta \rightarrow 0$, with $\delta = o(h^7)$.

TABLE 4. RBM error and computational time for various values of h , δ , and the expected error.

h	$\delta = h^{7/(1-\varepsilon)}$	Error RBM	Error Full-Graph	Execution time (s)		
				Discretize+RBM	Full-Graph	Speedup
5.00e-01	7.81e-03	2.3449e-01	2.6230e-01	159.95	156.79	0.98
3.33e-01	4.57e-04	1.4249e-01	3.0412e-01	198.28	241.72	1.22
2.50e-01	6.10e-05	9.4943e-02	3.0126e-01	231.97	337.06	1.45
2.00e-01	1.28e-05	6.7732e-02	2.8652e-01	265.68	431.90	1.62
1.43e-01	1.21e-06	3.9374e-02	2.4814e-01	331.14	605.40	1.83

4.2.2. *Nonoverlapping Decomposition.* In this example, we consider the same decomposition of the matrix \mathbf{R}_h introduced in (4.9), but with the following block matrices:

$$\mathbf{B}_1 = \begin{pmatrix} \mathbf{R}_h^1 & c_1^1 & 0 \\ a_1^1 & a_2^1 & a_3^1 & 1 & a_4^1 & 0 \\ 0 & c_2^1 & \overline{R_h} \end{pmatrix}, \mathbf{B}_2 = \begin{pmatrix} \overline{R_h} & 0 & c_1^2 & 0 & 0 \\ 0 & R_h & c_2^2 & 0 & 0 \\ a_4^2 & a_5^2 & 1 & a_6^2 & a_7^2 & a_8^2 \\ 0 & 0 & c_3^2 & \mathbf{R}_h^2 & 0 \\ 0 & 0 & 0 & 0 & \overline{R_h} \end{pmatrix}, \mathbf{B}_3 = \begin{pmatrix} \overline{R_h} & 0 & c_1^3 & 0 \\ 0 & R_h & c_2^3 & 0 \\ 0 & a_8^3 & a_9^3 & 1 & a_{10}^3 \\ 0 & 0 & c_3^3 & R_h \end{pmatrix}, \quad (4.13)$$

where the matrix \overline{R}_h is given by

$$\overline{R}_h = \left(\begin{array}{c|cc} R_1^* & 0 \\ \hline -1 & 1 \end{array} \right) \in \mathbb{R}^{\overline{N} \times \overline{N}}, \quad \underline{R}_h = \left(\begin{array}{cc|c} 1 & -1 & 0 \\ \hline -1 & & R_2^* \\ 0 & & \end{array} \right) \in \mathbb{R}^{N \times N}, \quad (4.14)$$

with $\overline{N} = (\lfloor N/2 \rfloor - 1)$, $\underline{N} = N - \overline{N} + 1$, and R_1^* and R_2^* being the square matrices R_h introduced in (2.7), but of sizes $(\overline{N} - 1) \times (\overline{N} - 1)$ and $(\overline{N} - 1) \times (\overline{N} - 1)$, respectively.

We observe that the matrix \overline{R}_h encodes the dynamics on half of an edge. In the present example, the block matrix \mathbf{B}_1 represents the dynamics on edges e_1 , e_2 , e_3 , and the first half of edge e_4 , while \mathbf{B}_2 corresponds to the dynamics on edges e_5 , e_6 , e_7 , the second half of e_4 , and edge e_8 . Finally, \mathbf{B}_3 captures the dynamics on edges e_9 , e_{10} , and the first half of e_8 (see Figure 5). We refer to this as a *non-overlapping decomposition* because the block matrices share dynamics only at a single discretization point. In contrast, the *overlapping decomposition* (presented in Section 4.2.1) features an overlap of N nodes (since the block matrices share a matrix of $N \times N$), so that the magnitude of shared information increases with N , whereas in the non-overlapping case, the shared information remains constant regardless of N .

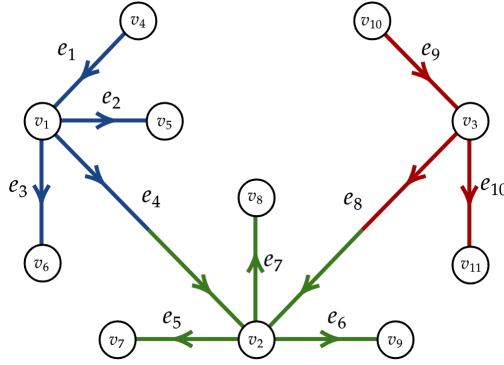


FIGURE 5. Illustration of the information contained in each block matrix. We illustrate in blue the information of \mathbf{B}_1 , in green the information of \mathbf{B}_2 , and in red the information of \mathbf{B}_3 .

Then, similar to (4.9), we introduce a decomposition of the matrix $\mathbf{R}_h = \mathbf{R}_1 + \mathbf{R}_2 + \mathbf{R}_3$ using the blocks \mathbf{B}_i introduced in (4.13). Furthermore, we decompose \mathbf{F}_h as

$$\mathbf{F}_h = (\mathbf{F}_1, 0, 0)^\top + (0, \mathbf{F}_2, 0)^\top + (0, 0, \mathbf{F}_3)^\top,$$

where

$$\mathbf{F}_1 = (\mathbf{f}_h^{e_1}, \mathbf{f}_h^{e_2}, \mathbf{f}_h^{e_3}, [\mathbf{f}_h^{e_4}]_{I_1})^\top, \quad \mathbf{F}_2 = ([\mathbf{f}_h^{e_4}]_{I_2}, \mathbf{f}_h^{e_5}, \mathbf{f}_h^{e_6}, \mathbf{f}_h^{e_7}, [\mathbf{f}_h^{e_8}]_{I_1})^\top, \quad \mathbf{F}_3 = ([\mathbf{f}_h^{e_8}]_{I_2}, \mathbf{f}_h^{e_9}, \mathbf{f}_h^{e_{10}})^\top. \quad (4.15)$$

Here, $I_1 = \{0, \dots, \overline{N}\}$ and $I_2 = \{\overline{N}, \dots, N\}$. Using (4.15), we define \mathbf{F}_{rb} according to (4.12), and \mathbf{R}_{rb} as in (2.9). Then, we introduce the system (4.11).

For the numerical simulation, we consider $N = 300$ elements for spatial discretization on each edge. To solve the ODEs, we use an implicit Euler scheme with $\zeta = 201$ time collocation points. To compute the expected value, we run 30 realizations. The numerical results are illustrated in Figure 6. Observe that the average approximates the solution on every edge, while the variance remains small. However, the *overlapping scheme* seems to be more accurate, at least on edges e_4 and e_8 .

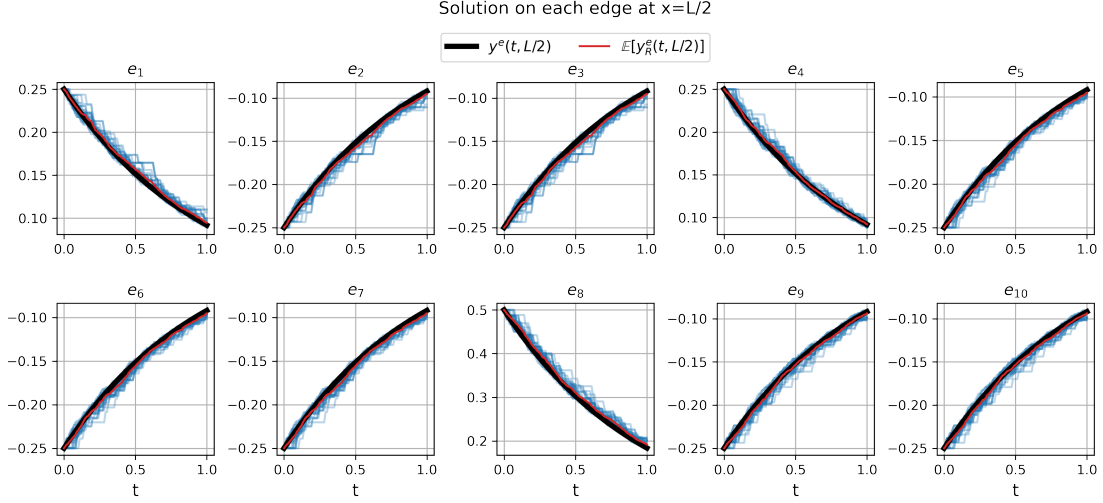


FIGURE 6. Comparison between the exact solution (in black) and the approximate solution at $x = L/2$ using the RBM (in red) on each edge with the *non-overlapping decomposition*. The blue lines represent the different realizations.

TABLE 5. Comparison of the (average) maximum memory usage, error, and (average) execution time between the discretize+RBM *non-overlapping* approach and the full-graph implicit Euler method. The error is computed using the L^∞ -norm in time and L^2 -norm in space for the full-graph method, and the L^∞ -norm in time and expected L^2 -norm in space for the discretize+RBM scheme.

Method	Memory usage (MB)	Error	Execution time (s)
Discretize+RBM	200.79	1.2896e-02	2.65
Full-Graph	510.33	9.6152e-03	8.56

Remark 4.1 (Computational Efficiency of RBM). *To explain why the RBM is computationally more efficient than solving the full system, we first note that the mass matrix \mathbf{E}_h has the same structure as the stiffness matrix \mathbf{R}_h . In both the overlapping and non-overlapping variants, when the submatrix \mathbf{R}_1 is selected on a subinterval (t_k, t_{k+1}) , the corresponding random system becomes*

$$\begin{pmatrix} E_{11}^1 & E_{12}^1 & 0 \\ E_{21}^1 & E_{22}^1 & E_{23}^1 \\ 0 & E_{32}^1 & E_{33}^1 \end{pmatrix} \partial_t \begin{pmatrix} \mathbf{Y}_R^1 \\ \mathbf{Y}_R^2 \\ \mathbf{Y}_R^3 \end{pmatrix} + \begin{pmatrix} \mathbf{B}_1/\pi_1 & 0 & 0 \\ 0 & 0 & 0 \\ 0 & 0 & 0 \end{pmatrix} \begin{pmatrix} \mathbf{Y}_R^1 \\ \mathbf{Y}_R^2 \\ \mathbf{Y}_R^3 \end{pmatrix} = \begin{pmatrix} \mathbf{F}_1/\pi_1 \\ 0 \\ 0 \end{pmatrix}. \quad (4.16)$$

Due to the block structure of this system, the only differential equation that needs to be solved is the reduced system

$$\pi_1 \left(E_{11} - E_{12} (E_{22} - E_{23} E_{33}^{-1} E_{32})^{-1} E_{21} \right) \partial_t \mathbf{Y}_R^1 + \mathbf{B}_1 \mathbf{Y}_R^1 = \mathbf{F}_1. \quad (4.17)$$

Although this system involves the inversion of a matrix, its size is strictly smaller than $N \times N$. That is, neither the system nor the matrices involved reach the full spatial dimension of the original problem. The remaining components of the solution can be obtained by

$$\mathbf{Y}_R^2(t) = \mathbf{Y}_R^2(t_k) - (E_{22} - E_{23} E_{33}^{-1} E_{32})^{-1} E_{21} (\mathbf{Y}_R^1(t) - \mathbf{Y}_R^1(t_k)), \quad (4.18)$$

and

$$\mathbf{Y}_R^3(t) = \mathbf{Y}_R^3(t_k) - E_{33}^{-1} E_{32} (\mathbf{Y}_R^2(t) - \mathbf{Y}_R^2(t_k)). \quad (4.19)$$

These expressions also involve matrix inversions; however, the required inverses are needed to solve (4.17). Therefore, besides the ones needed in (4.17), no additional matrix inversions are necessary.

In conclusion, the discretize+RBM scheme avoids the need to manipulate $N \times N$ matrices entirely. This structural advantage has been exploited in our implementation, leading to reductions in both memory usage and computational time.

Remark 4.2 (Non-overlapping Decomposition). We refer to the previous method as a non-overlapping decomposition due to its representation on the graph. However, classical non-overlapping domain decomposition, such as the Dirichlet-Neumann method, one imposes transmission conditions at interfaces to enforce flux continuity between adjacent subdomains. By contrast, the RBM splits the global stiffness matrix \mathbf{R}_h into submatrices as in (2.8), without introducing explicit interface operators.

Nonetheless, information does propagate across the subgraphs via the mass matrix couplings. Indeed, in the non-overlapping setting, in (4.16) when \mathbf{R}_1 is chosen on the time interval $[t_k, t_{k+1}]$, the only nonzero off-diagonal blocks of the mass matrix are rank-one. Concretely, in (4.16) one finds

$$E_{12} = \frac{h}{6} \mathbf{e}_{N_1} \mathbf{e}_1^\top, \quad E_{23} = \frac{h}{6} \mathbf{e}_{N_2} \mathbf{e}_1^\top, \quad E_{21} = \frac{h}{6} \mathbf{e}_1 \mathbf{e}_{N_2}^\top, \quad E_{32} = \frac{h}{6} \mathbf{e}_1 \mathbf{e}_{N_3}^\top, \quad (4.20)$$

where \mathbf{e}_i is the i -th canonical basis vector, and $N_1 = 3N + \bar{N} + 1$, $N_2 = 3N + \underline{N} + \bar{N}$ and $N_3 = 2N + \underline{N}$. Observe that the information spreads along the whole graph because (4.18) and (4.19). Moreover, in this case, the coupling into \mathbf{Y}_R^2 and \mathbf{Y}_R^3 is governed by \mathbf{Y}_{R,N_1}^1 , the N_1 -th component of \mathbf{Y}_R^1 . Namely,

$$\begin{aligned} \mathbf{Y}_R^2(t) &= \mathbf{Y}_R^2(t_k) - (E_{22} - E_{23} E_{33}^{-1} E_{32})^{-1} E_{21} (\mathbf{Y}_{R,N_1}^1(t) - \mathbf{Y}_{R,N_1}^1(t_k)) \\ &= \mathbf{Y}_R^2(t_k) - \frac{h}{6} (\mathbf{Y}_{R,N_1}^1(t) - \mathbf{Y}_{R,N_1}^1(t_k)) \left[\left(E_{22} - \frac{h^2}{36} \mathbf{e}_{N_2} (\mathbf{e}_1^\top E_{33}^{-1} \mathbf{e}_1) \mathbf{e}_{N_2}^\top \right)^{-1} \mathbf{e}_1 \right] \\ &=: \mathbf{Y}_R^2(t_k) - \frac{h}{6} (\mathbf{Y}_{R,N_1}^1(t) - \mathbf{Y}_{R,N_1}^1(t_k)) [\mathbf{T}^{-1} \mathbf{e}_1]. \end{aligned} \quad (4.21)$$

Similarly,

$$\begin{aligned} \mathbf{Y}_R^3(t) &= \mathbf{Y}_R^3(t_k) - E_{33}^{-1} E_{32} (\mathbf{Y}_R^2(t) - \mathbf{Y}_R^2(t_k)) \\ &= \mathbf{Y}_R^3(t_k) + \frac{h^2}{36} (\mathbf{Y}_{R,N_1}^1(t) - \mathbf{Y}_{R,N_1}^1(t_k)) [\mathbf{T}^{-1} \mathbf{e}_1]_{N_2} [E_{33}^{-1} \mathbf{e}_1], \end{aligned} \quad (4.22)$$

where $[\mathbf{T}^{-1} \mathbf{e}_1]_{N_2}$ denotes the N_2 -th component of $\mathbf{T}^{-1} \mathbf{e}_1$. Consequently, even when only \mathbf{R}_1 drives the evolution of (4.16), the rank-one entries in E_h ensure that the other components are never decoupled: each vector \mathbf{Y}_R^2 and \mathbf{Y}_R^3 is influenced by the boundary value \mathbf{Y}_{R,N_1}^1 . In this sense, the information is propagated through the entire graph. Furthermore, since $E_{ij} = O(h)$, both \mathbf{T}^{-1} and E_{33}^{-1} are $O(1/h)$, and therefore the propagation introduced by (4.21) and (4.22) persists even for small h .

Remark 4.3 (Comments on finite differences). The discretization using finite differences within each edge is analogous to the interval case. The discretization of the Neumann coupling conditions can be done by considering a first-order approximation using the boundary node and the previous one (inside the edge). Therefore, the discretization of the coupling conditions in (4.2) defines an algebraic equation, and thus, the discretization of (4.1)-(4.2) defines a differential-algebraic equation (DAE). Observe that the discretization at node v_1 leads to

$$4y_{(0)}^{e_4} = y_{(N)}^{e_1} + y_{(1)}^{e_2} + y_{(1)}^{e_3} + y_{(1)}^{e_4}. \quad (4.23)$$

At this point, the discretization does not align with the RBM presented in Section 2.2. However, by differentiating (4.23) with respect to time, we obtain the following differential equation representing the coupling condition:

$$\partial_t y_{(0)}^{e_4} = \frac{1}{4h} (4y_{(0)}^{e_4} - 2(y_{(N)}^{e_1} + y_{(1)}^{e_2} + y_{(1)}^{e_3} + y_{(1)}^{e_4}) + (y_{(N-1)}^{e_1} + y_{(2)}^{e_2} + y_{(2)}^{e_3} + y_{(2)}^{e_4})). \quad (4.24)$$

Assume that $y^0 \in H_0^1(\mathcal{E})$ also satisfies the Neumann condition in (4.2), then conditions (4.24) is equivalent to (4.23). Applying this to all interior vertices, we can express the discretization of (4.1)-(4.2) as a single ODE.

4.2.3. Optimal Control on a Graph. Let us consider the same graph \mathcal{G} introduced in the previous section. Denote by (y, f) the optimal pair of the optimal control problem (3.9) restricted to (4.1)-(4.2) (replacing the norms in $L^2(0, L)$ with norms in $L^2(\mathcal{E})$). In this section, we will use the Discretize+RBM methodology to approximate the optimal pair. Let us consider the discrete optimal control (3.10) restricted to (4.3), and denote its optimal pair as (y_h, f_h) . Due to [18], Theorem 3.2 holds for the optimal pairs (y, f) and (y_h, f_h) (replacing $L^2(0, L)$ with $L^2(\mathcal{E})$). Similar to (3.11), we observe that the vector of coefficient of (y_h, f_h) , satisfies the problem

$$\min_{\mathbf{F}_h \in L^2(0, T; \mathbb{R}^{10N+3})} \left\{ J_{\mathbf{E}_h}(\mathbf{F}_h) = \frac{1}{2} \int_0^T (\|\mathbf{F}_h(t)\|_{\mathbf{E}_h}^2 + \|\mathbf{Y}_h(t) - \mathbf{y}_{d,h}\|_{\mathbf{E}_h}^2) dt \right\}, \quad (4.25)$$

with \mathbf{Y}_h being the solution of (4.6), \mathbf{E}_h the mas matrix introduced in Section 4.1, and $\mathbf{y}_{d,h}$ the projection of y_d onto the space $V_h^\mathcal{E}$. Finally, consider the ω -dependent optimal control problem:

$$\min_{\mathbf{F}_R(\omega) \in L^2(0, T; \mathbb{R}^{10N+3})} \left\{ J_{\mathbf{E}_h}^R(\mathbf{F}_R(\omega)) = \frac{1}{2} \int_0^T (\|\mathbf{F}_R(t)\|_{\mathbf{E}_h}^2 + \|\mathbf{Y}_R(t) - \mathbf{y}_{d,h}\|_{\mathbf{E}_h}^2) dt \right\}, \quad (4.26)$$

where \mathbf{Y}_R is the solution of the random dynamics (4.11). Thus, by considering the projection of $(\mathbf{Y}_R, \mathbf{F}_R)$ into $V_h^\mathcal{E}$, we can conclude Theorem 3.3, in a complete analogous way. In the following, we will consider the *overlapping decomposition* and define R_{rb} as in Section 4.2.1.

The numerical solution of the optimal control problem (4.25) is obtained via a gradient-descent algorithm that solves the corresponding adjoint system to compute the gradient of the functional. To solve (4.26), we also employ the gradient-descent algorithm, with the adjoint equation solved using RBM. For both problems, we consider $N = 30$ and a uniform time discretization $\Delta t = T/(\zeta - 1)$, where $\zeta = 300$. The solution of each system is obtained using the implicit Euler scheme, wherein, for (4.26), the δ parameter of the RBM coincides with the time step used in the ODE discretization. For simplicity, we set $y_d = 1$. To compute the expectation of \mathbf{Y}_R , we perform 20 realizations and average the results.

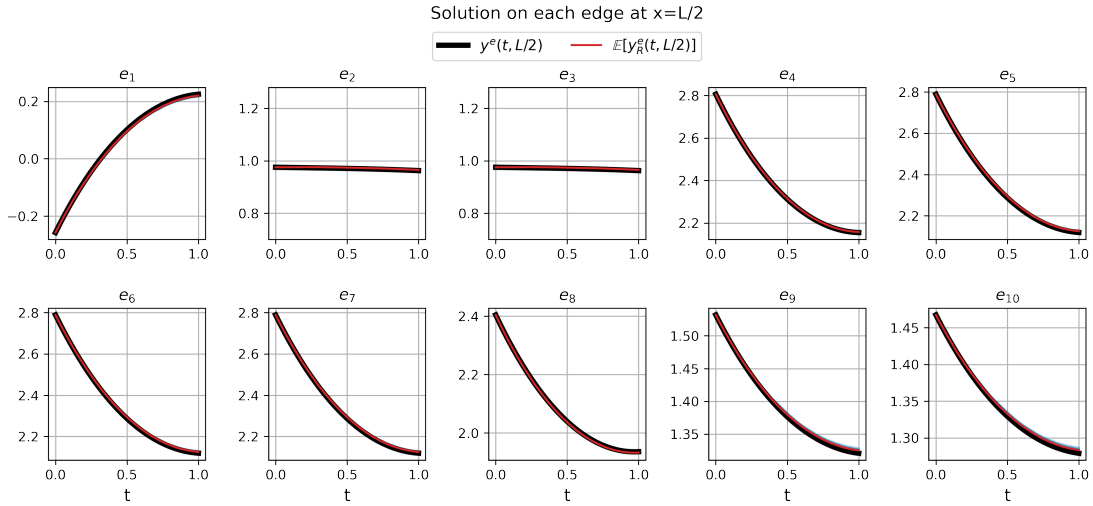


FIGURE 7. Comparison between the optimal state (in black) and the average optimal state at $x = L$ using the RBM (in red).

For both problems, the gradient descent tolerance is set to 10^{-8} ; that is, the iteration stops when the difference between consecutive controls is below 10^{-8} . Figures 7 and 8 display the optimal state and control, respectively, where the black curves denote the optimal solutions, and the red curves their RBM-based average.

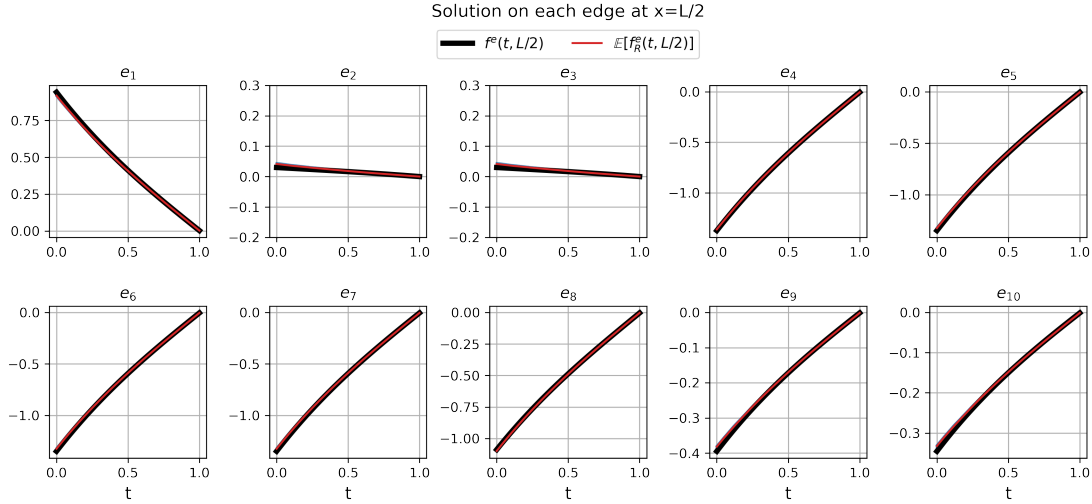


FIGURE 8. Comparison between the optimal control (in black) and the average optimal control at $x = L$ using the RBM (in red).

The expected optimal state and control of the random system closely approximate the true solutions. Table 6 summarizes the average maximum memory usage and execution time for solving (4.25) and (4.26). As noted in Section 4.2.1, the discretize+RBM method is both faster and more memory-efficient for the forward dynamics compared to the full-graph approach. Consequently, applying discretize+RBM to the adjoint state naturally accelerates the optimal control procedure. However, the memory usage for both problems is similar. One possible explanation is that the complete matrix \mathbf{E}_h is required during the gradient descent iterations for both cases.

TABLE 6. Comparison of average maximum memory usage and execution time between the discretize+RBM approach and the full-graph implicit Euler method for solving (4.25) and (4.26). The gradient descent algorithm terminates for both approaches when the error falls below $\epsilon - 8$.

Method	Memory usage (MB)	Execution time (s)
Discretize+RBM	125.44	358.96
Full-Graph	129.52	600.65

5. CONCLUSIONS AND OPEN PROBLEMS

In this paper, we develop and analyze the *discretize+RBM* method for fast and reliable computational approximation of the one-dimensional heat equation on graphs. We establish convergence of the method by carefully selecting the discretization and RBM parameters and analyzing the limit as they tend to zero.

We also illustrate our theoretical results with numerical experiments, where we observe that a suitable decomposition of the discrete system matrix exhibits behavior consistent with either overlapping or non-overlapping domain decomposition schemes, echoing classical techniques. These experiments for PDEs on graphs support our theoretical findings, demonstrating not only convergence but also a significant reduction in computational cost. This highlights the potential of the RBM as a versatile and efficient tool for solving and controlling PDEs on complex graph structures. Finally, we extend our analysis to the setting of optimal control.

Although this paper is devoted to the heat equation on graphs, this *discretize+RBM* approach can also be applied to higher-dimensional domains, as well as a broader class of linear PDEs. Indeed, once the PDE is discretized, a system similar to (4.6) is obtained.

In summary, for linear PDEs on graphs where computational efficiency is prioritized over exact precision, the Random Batch Method (RBM) provides a valuable solution. RBM enables the computation of approximate solutions more rapidly and with reduced memory requirements, while maintaining acceptable accuracy. This makes it particularly well-suited for applications such as gas network modeling.

Despite these findings, several open questions remain.

1) Extension of the Finite-Dimensional RBM: Although [31] provides a comprehensive analysis of RBM in finite-dimensional systems, there is currently no general theory for nonlinear ordinary differential equations (ODEs). RBM for nonlinear systems could be applied to power system models used in engineering that also involve graphs, such as Power Systems (see [22, Section 3.5]). Additionally, like the present study, RBM for nonlinear systems could be extended to nonlinear PDEs.

On the other hand, a natural question that arises when introducing (2.10) is whether it is possible to not only randomize the stiffness matrix R_h but also to randomize the mass matrix E_h . This is not straightforward since Remark 2.2 no longer holds, and the results in [31] cannot be directly applied. Therefore, a careful analysis is required to prove (or refute) the convergence when E_h is randomized.

2) Infinite-dimensional RBM: As shown in this article, it is possible to use the RBM techniques developed in [31] for ODEs and apply them in the context of PDEs, after spatial discretization.

It would be of interest to develop a RBM at the operator level, as in [7], but without relying on time discretization. Specifically, one could aim for a space-time continuous RBM for PDEs based on a randomized splitting of the operator generating the dynamics. Such an approach may yield convergence guarantees that are independent of the spatial discretization parameter h , depending only on the RBM parameter δ . Note that a true space-time continuous formulation cannot be inferred from [7], as their analysis ties the time-discretization, the implicit-Euler scheme, and the RBM parameter δ together.

Conversely, in the context of domain decomposition (see [20, Chapter III] and [27]), the transmission conditions prescribed at subdomain interfaces are both critical and scheme-dependent. In non-overlapping methods, one typically enforces Dirichlet–Neumann or Robin–Robin coupling to ensure stability and convergence, whereas overlapping Schwarz-type algorithms exploit the overlap width to dampen interfacial errors, imposing fewer constraints on boundary exchanges. In contrast, our approach omits explicit interface conditions because the RBM approximates the PDE through a discretized PDE, paying the price of taking $\delta = O(h^7)$ to ensure convergence. To avoid such dependence, it is necessary to directly approximate the PDE with a fully continuous RBM scheme. To this end, it is crucial to determine the precise interface laws that ensure the scheme’s well-posedness and convergence on average.

3) Graph Partitioning: In our numerical examples, we have demonstrated a partition inspired by overlapping and non-overlapping domain methods. However, since Theorem 3.1 holds for any splitting of the stiffness matrix R_h , the question naturally arises of identifying a graph partition that optimizes the approximation. Three strategies for graph decomposition that may be of interest are as follows. The first is based on *algebraic connectivity* or *Fiedler value*, namely, the second eigenvalue of the graph Laplacian, which quantifies the graph’s connectivity and enables a partition based on this measure. The second approach employs *machine learning* techniques, particularly the *Lloyd algorithm*—an iterative method (based on Voronoi diagrams) used to divide space into distributed regions. Although this method may serve as an initial step toward a partition that accelerates the RBM, it requires the incorporation of dynamic information. One possibility is to consider a weighted graph (with weights on the edges or vertices) that captures partial information about the solution at each time, and then apply the aforementioned techniques. Finally, as indicated in Remark 3.2, accelerating convergence requires minimizing the constant $C(M)$, which depends on the chosen splitting $\{R_m^h\}_{m=1}^M$. Therefore, for a fixed M , one may formulate an *optimization problem* to simultaneously minimize $C(M)$ and the l^1 (or l^0) norm of the matrices $\{R_m\}_{m=1}^M$, thereby promoting sparsity.

ACKNOWLEDGMENTS

The authors wish to express their gratitude to F. Hante and J. Giesselmann for their insightful discussions, and to S. Zamorano for taking the time to critically review the manuscript.

M. Hernández has been funded by the Transregio 154 Project, Mathematical Modelling, Simulation, and Optimization Using the Example of Gas Networks of the DFG, project C07, and the fellowship “ANID-DAAD bilateral agreement”. E. Zuazua has been funded by the Alexander von Humboldt-Professorship program, the European Research Council (ERC) under the European Union’s Horizon

2030 research and innovation programme (grant agreement NO: 101096251-CoDeFeL), the ModConFlex Marie Curie Action, HORIZON-MSCA-2021-DN-01, the COST Action MAT-DYN-NET, the Transregio 154 Project Mathematical Modelling, Simulation and Optimization Using the Example of Gas Networks of the DFG, AFOSR 24IOE027 project, grants PID2020-112617GB-C22 and TED2021-131390B-I00 of MINECO (Spain), and grant PID2023-146872OB-I00 of MICIU (Spain). Madrid Government - UAM Agreement for the Excellence of the University Research Staff in the context of the V PRICIT (Regional Programme of Research and Technological Innovation). Both authors have been partially supported by the DAAD/CAPIES grant 57703041 “Control and numerical analysis of complex systems”, and DFG and NRF. Südkorea-NRF-DKG-2023 programme, grant 530756074, and DASEL, Ciencia de Datos para Redes Eléctricas TED2021-131390B-I00/AEI/10.13039/501100011033.

REFERENCES

- [1] M. Badra and J.-P. Raymond. Approximation of feedback gains for abstract parabolic systems. *ESAIM Control Optim. Calc. Var.*, 31:Paper No. 17, 39, 2025.
- [2] C. Beisbart and N. J. Saam, editors. *Computer simulation validation*. Simulation Foundations, Methods and Applications. Springer, Cham, 2019. Fundamental concepts, methodological frameworks, and philosophical perspectives.
- [3] L. Bottou, F. E. Curtis, and J. Nocedal. Optimization methods for large-scale machine learning. *SIAM Rev.*, 60(2):223–311, 2018.
- [4] J. A. Carrillo, S. Jin, and Y. Tang. Random batch particle methods for the homogeneous Landau equation. *Commun. Comput. Phys.*, 31(4):997–1019, 2022.
- [5] A. D. Corella and M. Hernández. Mini-batch descent in semiflows. *ESAIM Control Optim. Calc. Var.*, 2025.
- [6] H. Egger and N. Philippi. On the transport limit of singularly perturbed convection-diffusion problems on networks. *Math. Methods Appl. Sci.*, 44(6):5005–5020, 2021.
- [7] M. Eisenmann and T. Stillfjord. A randomized operator splitting scheme inspired by stochastic optimization methods. *Numer. Math.*, 156(2):435–461, 2024.
- [8] L. C. Evans. *Partial differential equations*, volume 19 of *Graduate Studies in Mathematics*. American Mathematical Society, Providence, RI, second edition, 2010.
- [9] R. Glowinski, W. Kinton, and M. F. Wheeler. A mixed finite element formulation for the boundary controllability of the wave equation. *Internat. J. Numer. Methods Engrg.*, 27(3):623–635, 1989.
- [10] R. Glowinski and C. H. Li. On the numerical implementation of the Hilbert uniqueness method for the exact boundary controllability of the wave equation. *C. R. Acad. Sci. Paris Sér. I Math.*, 311(2):135–142, 1990.
- [11] R. Glowinski, C. H. Li, and J.-L. Lions. A numerical approach to the exact boundary controllability of the wave equation. I. Dirichlet controls: description of the numerical methods. *Japan J. Appl. Math.*, 7(1):1–76, 1990.
- [12] A. Iserles. *A first course in the numerical analysis of differential equations*. Cambridge Texts in Applied Mathematics. Cambridge University Press, Cambridge, second edition, 2009.
- [13] S. Jin and L. Li. On the mean field limit of the random batch method for interacting particle systems. *Sci. China Math.*, 65(1):169–202, 2022.
- [14] S. Jin, L. Li, and J.-G. Liu. Random batch methods (RBM) for interacting particle systems. *J. Comput. Phys.*, 400:108877, 30, 2020.
- [15] S. Jin, L. Li, and J.-G. Liu. Convergence of the random batch method for interacting particles with disparate species and weights. *SIAM J. Numer. Anal.*, 59(2):746–768, 2021.
- [16] D. Ko, S.-Y. Ha, S. Jin, and D. Kim. Uniform error estimates for the random batch method to the first-order consensus models with antisymmetric interaction kernels. *Stud. Appl. Math.*, 146(4):983–1022, 2021.
- [17] D. Ko and E. Zuazua. Model predictive control with random batch methods for a guiding problem. *Math. Models Methods Appl. Sci.*, 31(8):1569–1592, 2021.
- [18] M. Kroller and K. Kunisch. Convergence rates for the feedback operators arising in the linear quadratic regulator problem governed by parabolic equations. *SIAM J. Numer. Anal.*, 28(5):1350–1385, 1991.
- [19] D. Kulkarni, D. Schmidt, and S.-K. Tsui. Eigenvalues of tridiagonal pseudo-Toeplitz matrices. *Linear Algebra Appl.*, 297(1-3):63–80, 1999.
- [20] J. E. Lagnese and G. Leugering. *Domain decomposition methods in optimal control of partial differential equations*, volume 148 of *International Series of Numerical Mathematics*. Birkhäuser Verlag, Basel, 2004.
- [21] J. Latz. Analysis of stochastic gradient descent in continuous time. *Stat. Comput.*, 31(4):Paper No. 39, 25, 2021.
- [22] J. Machowski, Z. Lubosny, J. W. Bialek, and J. R. Bumby. *Power system dynamics: stability and control*. John Wiley & Sons, 2020.
- [23] D. Mugnolo. *Semigroup methods for evolution equations on networks*. Understanding Complex Systems. Springer, Cham, 2014.
- [24] L. Pareschi and M. Zanella. Reduced variance random batch methods for nonlocal PDEs. *Acta Appl. Math.*, 191:Paper No. 4, 23, 2024.
- [25] Y. Qiu, S. Grundel, M. Stoll, and P. Benner. Efficient numerical methods for gas network modeling and simulation. *Netw. Heterog. Media*, 15(4):653–679, 2020.
- [26] A. Quarteroni and A. Valli. *Numerical approximation of partial differential equations*, volume 23 of *Springer Series in Computational Mathematics*. Springer-Verlag, Berlin, 1994.

- [27] A. Quarteroni and A. Valli. *Domain decomposition methods for partial differential equations*. Numerical Mathematics and Scientific Computation. The Clarendon Press, Oxford University Press, New York, 1999. Oxford Science Publications.
- [28] Y. Shi, H. Fu, Y. Tian, V. V. Krzhizhanovskaya, M. H. Lees, J. Dongarra, and P. M. A. Sloot, editors. *Computational science—ICCS 2018. Part III*, volume 10862 of *Lecture Notes in Computer Science*. Springer, Cham, 2018. 18th International Conference, Wuxi, China, June 11–13, 2018.
- [29] F. Tröltzsch. *Optimal control of partial differential equations*, volume 112 of *Graduate Studies in Mathematics*. American Mathematical Society, Providence, RI, 2010. Theory, methods and applications, Translated from the 2005 German original by Jürgen Sprekels.
- [30] D. W. M. Veldman, A. Borkowski, and E. Zuazua. Stability and convergence of a randomized model predictive control strategy. *IEEE Transactions on Automatic Control*, pages 1–8, 2024.
- [31] D. W. M. Veldman and E. Zuazua. A framework for randomized time-splitting in linear-quadratic optimal control. *Numer. Math.*, 151(2):495–549, 2022.

Email address: martin.hernandez@fau.de

Email address: enrique.zuazua@fau.de